



Article

Validation of Expanded Trend-to-Trend Cross-Calibration Technique and Its Application to Global Scale

Ramita Shah¹, Larry Leigh^{2,*} , Morakot Kaewmanee² and Cibele Teixeira Pinto²

¹ Department of Electrical Engineering and Computer Science, South Dakota State University (SDSU), Brookings, SD 57007, USA

² Imaging Center, Image Processing Laboratory, Department of Electrical Engineering and Computer Science, South Dakota State University (SDSU), Brookings, SD 57007, USA

* Correspondence: larry.leigh@sdstate.edu; Tel.: +1-605-688-4161

Abstract: The expanded Trend-to-Trend (T2T) cross-calibration technique has the potential to calibrate two sensors in much less time and provides trends on a daily assessment basis. The trend obtained from the expanded technique aids in evaluating the differences between satellite sensors. Therefore, this technique was validated with several trusted cross-calibration techniques to evaluate its accuracy. Initially, the expanded T2T technique was validated with three independent RadCaTS RRV, DIMITRIPICS, and APICS models, and results show a 1% average difference with other models over all bands. Further, this technique was validated with other SDSU techniques to calibrate the newly launched satellite Landsat 9 with 8, demonstrating good agreement in all bands within 0.5%. This technique was also validated for Terra MODIS and ETM+, showing consistency within 1% for all bands compared to four PICS sites. Additionally, the T2T technique was applied to a global scale using EPICS Global sites. The expanded T2T cross-calibration gain result obtained for Landsat 8 versus Landsat 7/8, Sentinel 2A/2B, and Terra/Aqua MODIS presented that the difference between these pairs was within 0.5–1% for most of the spectral bands. Total uncertainty obtained for these pairs of sensors using Monte Carlo Simulation varies from 2.5–4% for all bands except for SWIR2 bands, which vary up to 5%. The difference between EPICS Global and EPICS North Africa was calculated using the ratio of trend gain; the difference among them was within 0.5–1% difference on average for all the sensors and bands within a 0.5% uncertainty level difference.

Keywords: EPICS Global; EPICS North Africa; T2T cross-calibration; Landsat 9; Landsat 8; Landsat 7; Aqua MODIS; Terra MODIS; Sentinel 2A; Sentinel 2B; Hyperion



Citation: Shah, R.; Leigh, L.; Kaewmanee, M.; Pinto, C.T. Validation of Expanded Trend-to-Trend Cross-Calibration Technique and Its Application to Global Scale. *Remote Sens.* **2022**, *14*, 6216. <https://doi.org/10.3390/rs14246216>

Academic Editors: Cody Anderson, Kathryn Ruslander, Michael Choate, Lawrence Ong and Esad Micijevic

Received: 19 October 2022

Accepted: 6 December 2022

Published: 8 December 2022

Publisher's Note: MDPI stays neutral with regard to jurisdictional claims in published maps and institutional affiliations.



Copyright: © 2022 by the authors. Licensee MDPI, Basel, Switzerland. This article is an open access article distributed under the terms and conditions of the Creative Commons Attribution (CC BY) license (<https://creativecommons.org/licenses/by/4.0/>).

1. Introduction

Monitoring the Earth from space has become routine; with the number of satellites increasing, monitoring them all for degradation is an ever-growing challenge [1]. Mechanical stress, cosmic rays, outgassing, and UV exposure during their operating life are a few of the reasons for satellite degradation. This deterioration in satellite performance impacts the satellite's pre-launch radiometric calibration, which also changes over time [2]. Therefore, continuous calibration monitoring is essential to obtain a precise and consistent radiometric measurement. Post-launch calibration also helps in ensuring the accuracy of data collected by the sensor. The radiometric calibration can be performed utilizing on-board calibrators like solar diffuser panels and lamps, among others [3,4].

On-board calibrators are an excellent way to ensure that the sensor delivers accurate data. However, not all satellites have on-board calibrators because of the increased cost. Furthermore, on-board calibration systems and sensors can degrade, so it requires performing the calibration utilizing other independent techniques [5]. Using satellite sensor imagery across a very stable area on the surface of Earth, known as Pseudo-Invariant Calibration sites (PICS), is a widely and alternative approach for calibration. PICS are

considered constant over time; thus, a change in the response of the sensor while imaging PICS sites can be attributed to changes in the sensor itself rather than a change in the target [6,7]. Several desert sites were determined as temporally, spatially, and spectrally stable sites for calibration. The Committee on Earth Observation Satellites (CEOS) chose six desert regions in North Africa as the stable sites used internationally. These six African desert sites are Algeria 3, Algeria 5, Libya 1, Libya 4, Mauritania 1, and Mauritania 4 [8,9].

For many years, PICS has been utilized for the calibration of many optical instruments on board Earth observation satellites. The number of clear, usable scenes, however, considerably decline due to environmental conditions like sandstorms and clouds, the field of view of the sensor, and temporal resolution over these stable PICS [10]. This results in a reduced dataset to perform radiometric calibration of the sensor and, in turn, takes more time to build up a dense dataset. To overcome the temporal resolution issue using traditional stable PICS, Vuppula et al. [10] developed a cross-calibration method that combines data from six PICSs in North Africa acquired by Landsat 8 as a single dataset. In what the author referred to as the “PICS Normalization Process,” where Egypt 1, Libya 1, Libya 4, Niger 1, Niger 2, and Sudan 1 sites were normalized, considering Libya 4 as a reference site. The author reported a dense dataset and an improvement in the temporal resolution in PICSs for Landsat 8 and was also able to collect observations in 3–4 days, an improvement from the normal 16 days.

Even though the temporal resolution was significantly increased through the combination of traditional PICS, this technique was unable to achieve daily observation. Daily observations may help in faster detecting long-term changes in the response of the sensor and addressing them sooner. Daily observations can also be utilized to identify irregular short-term changes in the sensor that could otherwise go undetected. Shrestha et al. [11,12] attempted to achieve nearly daily acquisitions by developing a characterization of North Africa in an effort to find spatially, temporally stable, and spectrally similar regions across the continent instead of utilizing specific regions as in the traditional PICS technique. North Africa’s spectral response was used to perform classification based on both the sites’ temporal stability and their spectral features, along with their temporal stability characterization. This classification resulted in the identification of 19 “clusters” across North Africa; due to its spatial response, temporal features, and spectral response, “Cluster 13” of 19 “cluster” was chosen as a potential candidate for an Extended PICS (EPICS). Hasan et al. [13] demonstrated that EPICS could offer cloud-free observations almost daily with “Cluster 13” of 19 “cluster” in North Africa (EPICS North Africa).

In a traditional cross-calibration method, coincident and near-coincident scenes were used to perform calibration, which requires more time to acquire a dense dataset for short-term and long-term trend analysis. Cross-calibration using EPICS can solve traditional cross-calibration due to its potential to provide scenes on a near-daily basis. Khakurel et al. [14] presented a new T2T cross-calibration technique to overcome this limitation of the traditional cross-calibration method. The author used EPICS North Africa to cross-calibrate two sensors, as the cluster-based approach helped to obtain near-daily observations. This technique can obtain trend gains on a daily basis, which is a key advantage that allows for determining sensor performance by analyzing the short-term and long-term trends of the temporal dataset. The T2T technique can be utilized to calibrate two sensors in a much shorter time frame with the same level of accuracy as traditional methods. This technique can be very useful in calibrating the newly launched satellite’s sensor within a significantly shorter time compared to any other cross-calibration technique, as the model can predict observations on a daily basis.

As explained above, EPICS North Africa has the potential to provide observations on a daily basis; however, multiple observations per day can help in achieving a denser dataset in the same time frame compared to EPICS, enabling faster evaluation of sensor performance. Fajardo et al. [15] expanded the 19 “cluster” classification to a global scale with a motive to achieve multiple observations per day. The author successfully developed a “160 Class Global Classification” with global coverage, which includes 23 World Reference

System (WRS-2) paths/rows. The EPICS Global could achieve multiple observations per day with similar spectral characteristics and still produce a temporal coefficient of less than 4% variation for all bands compared to the traditional PICS. EPICS Global enhanced the potential of calibrating optical satellite sensors, minimizing the possible variability of a single calibration site. Later, this classification was improved by “300 global class classifications”, including 33 optimal WRS-2 path/row locations throughout the globe. This work demonstrated that EPICS Global could be useful in performing calibration in a short period to evaluate the performance of the newly launched satellite and monitor its stability.

After the development of the EPICS global, it could be more efficient to cross-calibrate sensors using multiple images per day. For this reason, a newly developed T2T cross-calibration technique can be further analyzed and modified to become a powerful technique for calibrating the newly launched satellite’s sensor, as this technique can obtain scenes on a daily basis and give temporal trends. The primary goal of this work is to expand the T2T cross-calibration technique to see the sensors’ temporal trend, which gives a sense of the sensor’s performance. The expanded T2T technique is evaluated through its comparison with several trusted cross-calibration techniques to determine the accuracy of this technique. Additionally, the expanded T2T cross-calibration technique is applied on a global scale using EPICS global, with the potential of acquiring multiple observations per day.

2. Sensor Used

Khakurel et al. [14] used Landsat 7, Landsat 8, Sentinel 2A, and Sentinel 2B sensors to perform T2T cross-calibration by making possible pairs. Terra MODIS and Aqua MODIS are added to this work to evaluate the potential and diversity of techniques to handle different Earth observation sensors. These sensors have been acquiring observations for many years and are frequently utilized for calibration. However, Landsat 9 was also used in this work to demonstrate the potential of the expanded T2T cross-calibration technique to calibrate the newly launched satellite sensor after a week in orbit.

2.1. Landsat Series

Landsat 7 has been acquiring images of the Earth since April 1999 and has an Enhanced Thematic Mapper Plus (ETM+) sensor. It has eight spectral bands, among which one is a panchromatic band with 15 m resolution and seven bands with 30 m spatial resolution, with a repeating cycle of 16 days [16]. Since May 2003, Landsat 7 has been facing a problem with Scan Line Corrector (SLC), causing scenes collected with wedge-shaped data gaps [17]. ETM+ on-orbit radiometric stability is tracked utilizing vicarious measurements and on-orbit calibration combinations. The onboard calibrators regularly use the sun as a radiation source for partial and full-aperture solar calibration [18].

Landsat 8 satellite was launched on 11 February 2013, which has the Operational land manager (OLI) and the thermal infrared sensor (TIRS) instruments. This satellite completes its orbital cycle every 16 days, located at an altitude of 705 km on a sun-synchronous orbit. The OLI sensor measures solar reflectance at 30 m spatial resolutions in eight spectral bands and 15 m spatial resolutions in the panchromatic band. Landsat 8 is designed with its push broom architecture. All focal planes contain over 69,000 detectors spread through 14 separate modules, enabling them to image a large swath of 185 km corresponding to a 15 degrees field of view [3,19].

Landsat 9, launched on 27 September 2021, is an Earth observation satellite that carries the Operational Land Imager 2 (OLI-2) and Thermal Infrared Sensor 2 (TIRS-2). Landsat 9 onboard instruments are improved replicas of Landsat 8 onboard devices currently collecting geometrically and radiometrically superior data compared to the previous generation of Landsat satellites. This satellite enhancement includes higher radiometric resolution, such as a 14-bit quantization increased from 12-bit compared to Landsat 8, which allows the sensor to detect more subtle differences. This satellite is located at a 705 km altitude in the sun-synchronous orbit and completes the orbital cycle in 16 days [16].

2.2. Aqua/Terra MODIS

Moderate Resolution Imaging Spectroradiometer (MODIS) is a key instrument aboard the Aqua (EOS PM) and Terra (EOS AM) satellites. In the morning, Terra MODIS orbits around the Earth such that it passes from north to south across the equator, whereas Aqua MODIS passes from south to north in the afternoon. Both satellites view the surface of the entire Earth every two days. These satellites have 36 spectral bands with wavelengths ranging from 0.41–14.5 μm . MODIS is placed at 705 km altitude in a sun-synchronous orbit with a spatial resolution of 250 m for bands 1–2500 m for bands 3–7, and 1000 m for bands 8–36 [20,21].

2.3. Sentinel 2A/2B MSI

Sentinel 2A and Sentinel 2B were launched on 23 June 2015 and 7 March 2017. These satellites are phased at 180 degrees to each other, consist of a push-broom sensor multispectral instrument (MSI), and are placed at an altitude of 786 km in a sun-synchronous orbit. Sentinel 2A/2B measures solar reflectance across 13 spectral bands with spatial resolutions of 10 m, 20 m, and 30 m. These two satellites complete one rotation of Earth in 10 days and together in 5 days. The Sentinel MSI focal plane detectors are spread across 12 different modules, allowing these satellites to image at a field of view of 20.6 degrees and a swath of 290 km [22,23].

Table 1 shows the further comparison of Landsat 7, 8, and 9, Sentinel 2A/2B, and Aqua/Terra MODIS using their characteristics such as launch date, bands, spatial resolution, equatorial crossing time, swath width, and so on.

Table 1. Characteristics comparison of sensors used for expanded T2T cross-calibration Technique.

Characteristics	Sensors			
	Landsat 8/9	Landsat 7	Sentinel 2A/2B	MODIS Terra/Aqua
Launch Date	11 February 2012/ 27 September 2021	15 April 1999	23 June 2015/ 7 March 2018	18 December 1999/ 4 May 2002
Number of Bands	11 (1 pan, 8 multispectral, 2 thermal)	8 (1 pan, 6 multispectral, 1 thermal)	13 (All multispectral)	36 (Spectral Bands)
Spatial Resolution	15, 30, 100 (m) (pan, multispectral, thermal)	15, 30, 60 (m) (pan, multispectral, thermal)	10, 20, 60 (m) (All multispectral)	250, 500, 1000 (m) (Bands 1–2, 3–7, 8–36)
Equatorial crossing time	10:00–10:15	10:00–10:15	10:30	10:30
Swath width	183 (km)	183 (km)	290 (km)	2330 (km)
Revisit frequency	16 (days)	16 (days)	10 (days)	1–2 (days)
Orbit altitude	705 (km)	705 (km)	785 (km)	705 (km)

3. Methodology

An extended T2T cross-calibration technique has been developed in this paper with significant modifications to the T2T cross-calibration technique by Khakurel et al. [14]. The Section 3 shows the improvements made to the T2T cross-calibration technique so that this approach can be applied to the global scale and give consistent results compared to other trusted cross-calibration models. Figure 1 shows the steps used to develop the expanded T2T cross-technique for global application. This section describes the expanded T2T cross-calibration technique's development.

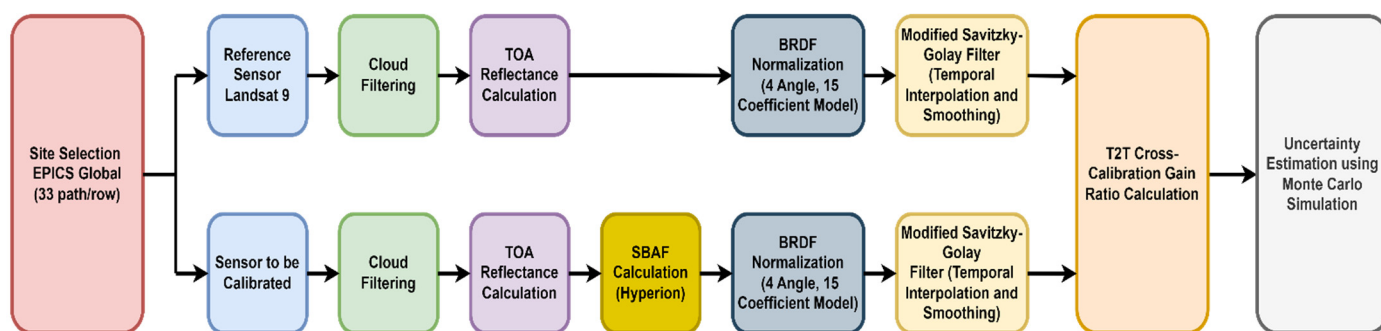


Figure 1. Workflow Diagram used for trend-to-trend Cross-calibration using Global EPICS.

3.1. Site Selection

Khakurel et al. [14] used EPICS North Africa cluster to perform cross-calibration with the newly proposed T2T technique due to the potential of this cluster to collect nearly daily observations. Using clusters, the author was able to calibrate sensors on a daily basis and gave the temporal cross-calibration factor, which helped in analyzing sensor performance. To expand the application of the T2T cross-calibration technique, this approach is applied to a global scale by using EPICS global, which can provide multiple observations per day. Trend, drift, and changes in sensor performance can be detected quicker with lower Uncertainty using EPICS global through more images. Another motive for using a global cluster was to apply and evaluate expanded T2T cross-calibration techniques when applied to the newly launched Landsat 9. Figure 2a–e presents EPICS Global stable pixels over North Africa, Middle East, Central Africa, Australia, and North America, along with the Landsat 8 scenes.

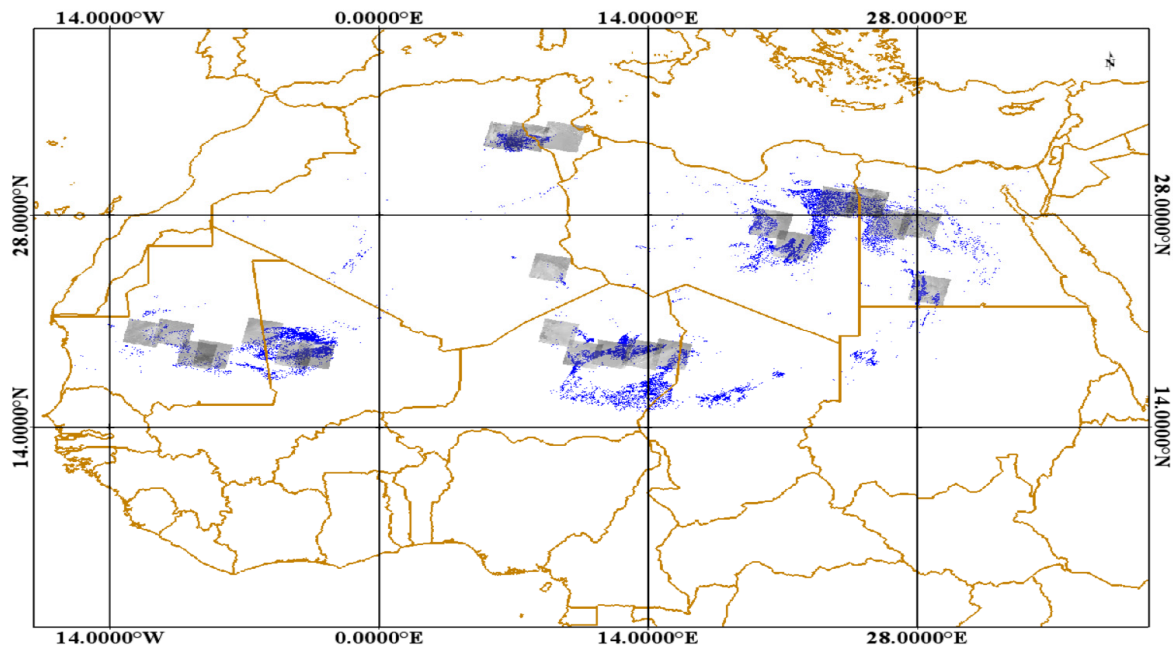
3.2. Cloud Screening from Scenes

After selecting a site for this work, images from all the sensors used for this purpose were extracted. Calibration can only be done in cloud-free images, which is necessary to remove cloudy pixels from the images. Cloudy pixels from the scenes were determined using different techniques for different satellite sensors before calculating the TOA reflectance. For all the selected sensors, such as Landsat 7, Landsat 8, Landsat 9, Sentinel 2A, Sentinel 2B, Aqua MODIS, and Terra MODIS, images with more than 50 percent cloudy and cloud shadow pixels were discarded from further analysis.

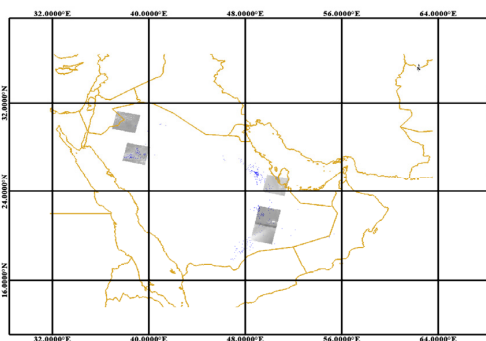
For ETM+, Landsat 8 and Landsat 9 level 1 collection 2 Pixel Quality Assessment Band was used to make cloud filtering masks from the scenes. Landsat level 1 collection 2 Quality Assessment bands provide helpful information to the users willing to optimize the pixel value as the first level indicator of different information within the Landsat dataset. QA_PIXEL bands files have quality statistics collected using the image data along with the cloud filter mask information for the images. Bit 0 (fill values), Bit 1 (Dilated Cloud), Bit 2 (Cirrus), Bit 3 (Cloud), Bit 4 (Cloud Shadow), Bit 9 (Cloud Confidence), Bit 11 (Cloud Shadow Confidence), and Bit 15 (Cirrus Confidence) were used to make cloud filtering masks. The bits details for Level 1 collection 2 products of Landsat the series were obtained from the United States Geological Survey (USGS) website (<https://www.usgs.gov/landsat-missions/landsat-collection-2-quality-assessment-bands>), accessed on 23 September 2021.

For both Terra and Aqua MODIS, Collection 6.1 image data product was accessed from MODAPS Web services (<https://modwebsrv.modaps.eosdis.nasa.gov/>) accessed on 2 March 2022. The projection used for the cloud mask product for Collection 6.1 image data product is in a sinusoidal projection (https://lpdaac.usgs.gov/documents/715/MOD11_User_Guide_V61.pdf), accessed on 15 December 2021. However, our local archive image data product is in UTM projection. Therefore, band 26 was used to create a cloud mask to filter cloudy pixels from scenes [24]. For each resolution, a binary cloud mask was created for the Sentinel dataset to filter out the cloudy pixels from the images. Zone-specific zonal masks were made to extract EPICS global pixels from the 33 paths/rows of images. These

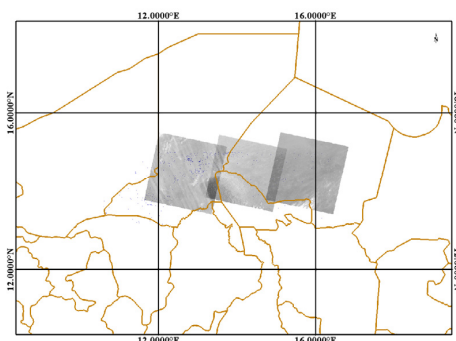
zonal masks were created using the methodology used by Hasan [13] to create zone-specific zonal masks for cluster 13 of 19 “cluster” classification to extract pixels of the cluster that lie on the selected paths/rows observations.



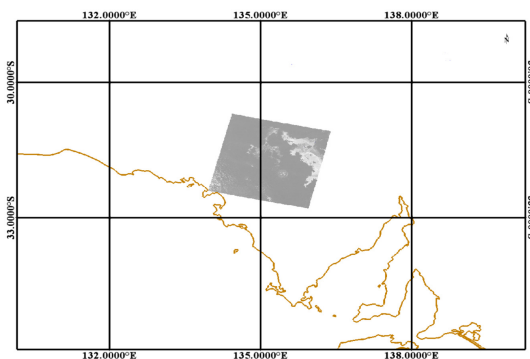
(a)



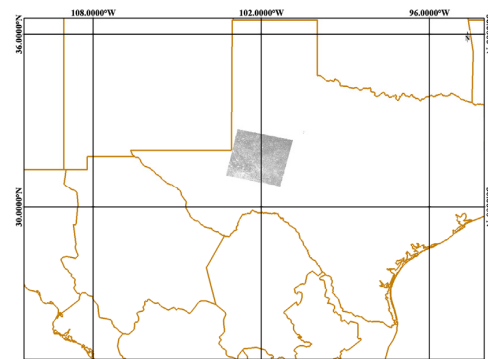
(b)



(c)



(d)



(e)

Figure 2. (a–e) Shows Global EPICS pixel over North Africa, Middle East, Central Africa, Australia, and North America along with the Landsat 8 scenes.

3.3. TOA Reflectance Computation

After removing the clouds in scenes, the image data is measured in unitless DN numbers, which need to be converted into NIST traceable that are consistent units, in this case, Top of Atmosphere (TOA) reflectance calculation. This section explains the equations for TOA reflectance computation for all the sensors used in the analysis.

3.3.1. Landsat Series TOA Reflectance

For ETM+, Landsat 8, and Landsat 9 rescaling coefficient from the metadata file was used to calculate TOA reflectance using Equation (1).

$$\text{TOA_Reflectance } (\rho_{\lambda}) = \frac{M\rho \times Q_{\text{Cal}} + A_P}{\cos(\theta_{\text{SZ}})} \quad (1)$$

where ρ_{λ} is TOA reflectance for level 1 collection 2 product with cosine correction of solar zenith angle; Q_{Cal} is the calibrated and quantized product pixel value; $M\rho$ is the band-specific multiplicative factor and A_P is additive factor obtained from the metadata file; and θ_{SZ} is the per-pixel solar zenith angle obtained from the solar angle band.

3.3.2. MODIS TOA Reflectance

TOA reflectance of Terra and Aqua MODIS can be computed using Equation (2).

$$\text{TOA_Reflectance } (\rho_{\lambda}) = \frac{Q_{\text{Cal}}}{\cos(\theta_{\text{SZ}}) \times k} \quad (2)$$

where ρ_{λ} is TOA reflectance for collection 6.1 products of Aqua and Terra MODIS; Q_{Cal} is the calibrated and quantized product pixel value; θ_{SZ} is the per-pixel solar zenith angle obtained from the solar angle band, and k is the quantization value or reflectance scaling factor obtained from the metadata file.

3.3.3. Sentinel TOA Reflectance

For sentinel 2A and Sentinel 2B sensors, there are two methods for TOA reflectance calculation because of the processing differences. TOA reflectance calculation of the MSI before this date, 20220125, can be calculated using Equation (3).

$$\text{TOA_Reflectance } (\rho_{\lambda}) = \frac{Q_{\text{Cal}}}{k} \quad (3)$$

where ρ_{λ} is TOA reflectance for Sentinel Level1; Q_{Cal} is the calibrated and quantized product pixel value, and k is the quantization value or reflectance scaling factor obtained from the metadata file.

Dataset obtained after 20220125 date for both sentinel 2A and Sentinel 2B sensors, TOA reflectance was calculated using Equation (4).

$$\text{TOA_Reflectance } (\rho_{\lambda}) = \frac{Q_{\text{Cal}} + \text{RADIO_ADD_OFFSET}}{k} \quad (4)$$

where ρ_{λ} is TOA reflectance for Sentinel Level1; Q_{Cal} is the calibrated and quantized product pixel value, and k is the quantization value or reflectance scaling factor RADIO_ADD_OFFSET is the radiometric offset. In addition, these parameters are obtained from the metadata file.

3.4. SBAF Calculation Using Hyperion

Satellites do not see the planet the same way due to spectral band differences. While performing cross-calibration between satellite sensors, the response can be different when they look at the same target, even if they are perfectly calibrated due to this spectral difference. To correct these spectral differences, a factor is computed to adjust the spectral response to two satellite sensors. This factor is referred to as the Spectral Band Adjustment

Factor (SBAF). The SBAF is calculated using the spectral profile of the target from Hyperion and the relative spectral response (RSR) of the satellite's sensors. In T2T cross-calibration technique, a sensor pair was calibrated considering one reference sensor, which is assumed to be well calibrated, and another one as a sensor selected for calibration [6]. SBAF value is applied to the sensor selected for calibration to match its response with the reference sensor. The equation used for SBAF computation is given below.

$$\text{SBAF} = \frac{\rho_{\lambda(\text{reference_sensor})}}{\rho_{\lambda(\text{Target_sensor})}} = \frac{\int \rho_{\lambda h} \text{RSR}_{\lambda(\text{ref})} d\lambda}{\int \text{RSR}_{\lambda(\text{ref})} d\lambda} \frac{\int \text{RSR}_{\lambda(\text{cal})} d\lambda}{\int \rho_{\lambda h} \text{RSR}_{\lambda(\text{cal})} d\lambda} \quad (5)$$

$$\rho'_{\lambda(\text{Target_sensor})} = \text{SBAF} \times \rho_{\lambda(\text{Target_sensor})} \quad (6)$$

where $\rho_{\lambda(\text{reference_sensor})}$ and $\rho_{\lambda(\text{Target_sensor})}$ are simulated TOA reflectance for the reference sensor and sensor chosen for calibration, respectively; $\rho_{\lambda h}$ is surface hyperspectral profile; $\text{RSR}_{\lambda(\text{ref})}$ is the RSR response of the reference sensor and $\text{RSR}_{\lambda(\text{cal})}$ is the RSR response of the sensor selected for calibration.

The RSR of the multispectral sensor is integrated at each sampled wavelength with the hyperspectral profile of the target to obtain simulated TOA reflectance. Equation (6) shows the application of calculated SBAF values to the sensor selected for calibration to match its reflectance with the reference sensor. Where $\rho'_{\lambda(\text{Target_sensor})}$ is the TOA reflectance of the sensor selected for calibration, which is scaled equivalent to the reference sensor TOA reflectance, and $\rho_{\lambda(\text{Target_sensor})}$ is the original TOA reflectance of the sensor that needed to be calibrated.

EO-1 Hyperion data from USGS EarthExplorer (<https://earthexplorer.usgs.gov/>, accessed on 1 December 2018) is used for obtaining the spectral profile of the target over EPICS Global. As explained in Shrestha et al., a scene containing more than 10% cloudy pixels and scenes with 5 degrees or more look angles were discarded [25]. Using EPICS North Africa, Khakurel et al. [14] obtained 213 hyperspectral images, whereas using EPICS Global, a total of 2300 hyperspectral images were obtained as all the path/row intersecting cluster pixel was used. These images were drift-corrected with absolute gain and bias correction [26]. Obtaining significantly more hyperspectral images helped in better estimating SBAF values for cross-calibration. Figure 3 is the hyperspectral profile obtained from Hyperion for EPICS Global cluster. The SBAF-applied sensor and reference sensor were BRDF normalized in the next section.

3.5. BRDF Normalization

Datasets acquired from earth observation sensors have variability in their TOA reflectance because of factors like sun position, atmospheric effects, acquisition viewing geometry, and so on. The bidirectional reflectance distribution function (BRDF) of the target is one of the major contributors to TOA reflectance variability. The BRDF variability is mostly driven by the drastic change in the sun's position throughout the different seasons in a year, and the view geometry for these nadir sensors is expected to be consistent. Additionally, an increase in the sensor's field of view and variation in orientation among the sensors imaging the same target with the same solar position also increases the BRDF effect [27]. Hence, for further analysis, all the sensors used for this work must be BRDF normalized to the same reference angle.

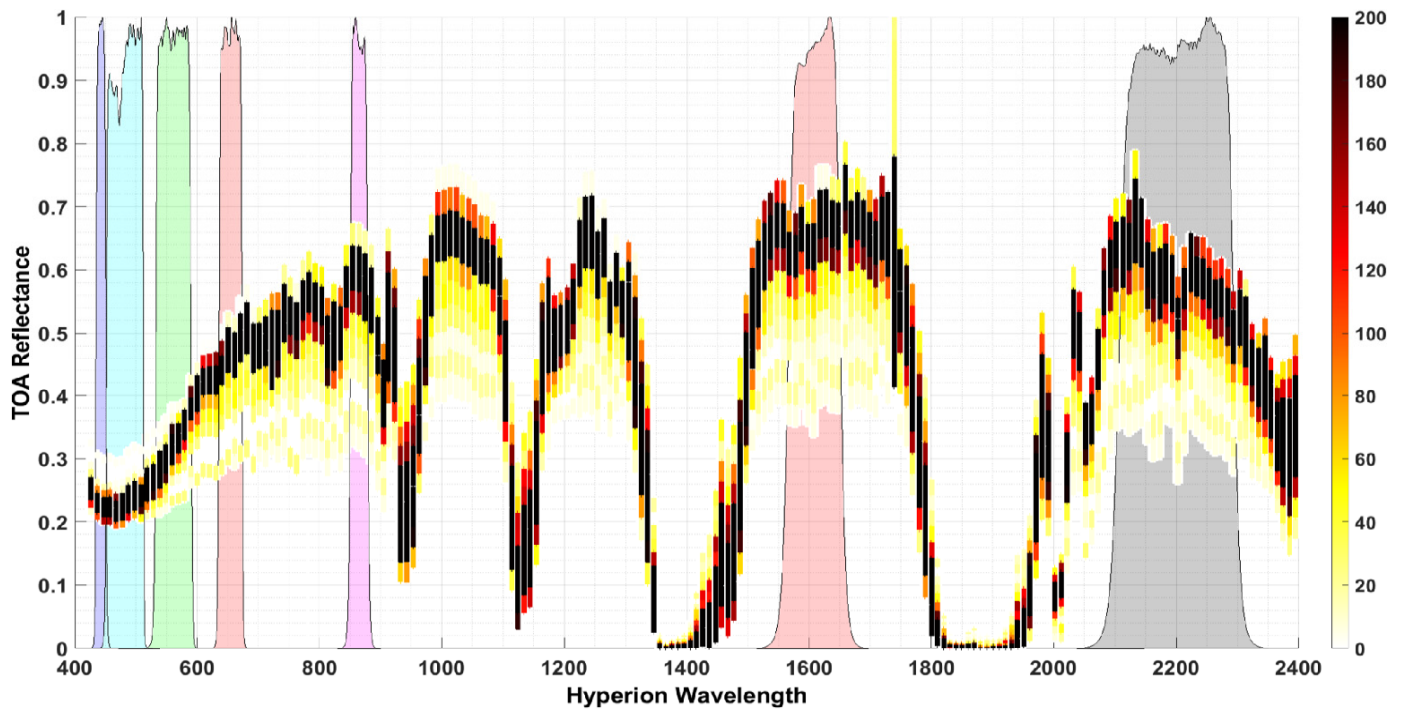


Figure 3. Hyperspectral profile of EPICS Global Data using Hyperion and shaded reason shows RSR for Landsat 8.

Libya 4 site has been used to develop an absolute calibration BRDF model, which derives quadratic and linear functions of the solar zenith angle [28]. Farhad et al. [29] derived the BRDF model incorporating four angles to properly account for the effect and variability of BRDF. This model provides a TOA reflectance of the surface as a continuous function of independent variables by converting the view and solar angles from a spherical coordinate to a linear Cartesian basis. The BRDF model developed by Farhad was further expanded by Kaewmanee [30] through better interaction terms that better characterized the BRDF model and better uncertainty after the normalization of the dataset. Kaewmanee used the 15-coefficient quadratic model given below.

$$\rho_{\text{Predicted_Model}} = \beta_0 + \beta_1 X_1 + \beta_2 Y_1 + \beta_3 X_2 + \beta_4 Y_2 + \beta_5 X_1 Y_1 + \beta_6 X_1 X_2 + \beta_7 X_1 Y_2 + \beta_8 Y_1 X_2 + \beta_9 Y_1 Y_2 + \beta_{10} X_2 Y_2 + \beta_{11} X_1^2 + \beta_{12} Y_1^2 + \beta_{13} X_2^2 + \beta_{14} Y_2^2 \quad (7)$$

$$X_1 = \sin(\text{SZA}) * \cos(\text{SAA}) \quad (8)$$

$$X_2 = \sin(\text{VZA}) * \cos(\text{VAA}) \quad (9)$$

$$Y_1 = \sin(\text{SZA}) * \sin(\text{SAA}) \quad (10)$$

$$Y_2 = \sin(\text{VZA}) * \sin(\text{VAA}) \quad (11)$$

$$\rho_{\text{BRDF_Normalized_Reflectance}} = \frac{\rho_{\text{Observed_Reflectance}}}{\rho_{\text{Predicted_Reflectance}}} * \rho_{\text{Reference_Geometry}} \quad (12)$$

where, $\beta_0, \beta_1, \dots, \beta_{14}$ are 15 coefficients used by the model, and $X_1, X_2, Y_1,$ and Y_2 are the Cartesian coordinates showing the planar projection of the sensor and solar angles, which was initially in the spherical coordinate. SAA and SZA are the solar azimuths and zenith angles, and VAA and VZA are view azimuth and zenith angles, respectively. $\rho_{\text{Observed_Reflectance}}$ is the observed TOA reflectance for each cloud-filtered scene; $\rho_{\text{Predicted_Reflectance}}$ is the TOA reflectance predicted by the model for each observation, and $\rho_{\text{Reference_Geometry}}$ is the reference TOA reflectance generated by using the same reference geometry. Reference geometry contains solar and sensor angles described by Fajardo. In order to normalize the TOA reflectance to acquisition geometry with real obtained angles

from the scene that offer reflectance similar to the mean of the cluster, the reference solar and sensor angles were chosen in the dataset's center. The same reference angles were used for all the sensors for the BRDF normalization process to normalize them to the same scale.

3.6. Temporal Interpolation Using MSG Filter

After BRDF normalizing the dataset for both the reference sensor and sensor selected for calibration, it was necessary to obtain a trend line to see the temporal trend, as the major motive of this approach was to calibrate sensors on a daily basis. For this reason, the T2T cross-calibration approach uses a Modified Savitzky-Golay (MSG) filter for trend identification and data smoothing. Savitzky and Golay proposed the Savitzky-Golay filter, a time-domain method to smooth data using a low pass filter based on approximating the local least-square polynomial [31]. MSG filter has the potential to preserve the peak shape property of the dataset and generate a dataset on a daily basis with significant patterns presented in the original data [32]. The following equation can be used to determine the polynomial function.

$$f(a) = C_0 + C_1 a + C_2 a^2 + \dots + C_n a^n \quad (13)$$

where C is the set of coefficients and n is the polynomial degree. While using the MSG filter, the polynomial is fit to the given dataset for the specific window size, producing an output and giving the polynomial value at the window's central point. Likewise, the next point can be obtained by shifting the window by a day and repeating the process until the point for each day is determined.

Khakurel et al. used an MSG filter with 60 days window size with polynomial order three for the North African continent as this window size gave the best estimation for the dataset to determine temporal trend. In expanded T2T cross-calibration technique, MSG filter with 120 days window size, polynomial order three, normalize and robust feature. The reason for choosing 120 days window size was to see the major seasonal changes in the dataset if they exist, as there are three major seasons in a year, consisting of spring, summer, and fall. These seasons are mostly considered to be constant for EPICS global pixels because all the pixels in the clusters represent sand or desert. The four-month window size was used to smooth the dataset further and temporally fill the dataset with more significant gaps. A normalized and robust feature was added to the filter to center and scale the data set and a robust linear least-square fitting method.

3.7. Expanded T2T Cross-Calibration Gain

Expanded T2T cross-calibration gain was obtained using the trends of both sensors after MSG smoothing T2T cross-calibration. T2T cross-calibration gain helps to obtain the temporal difference between the reference sensor and sensor used for calibration on a daily basis and gives a sense of the short-term and long-term trend useful for determining sensors performance. The trend gain was calculated by taking the ratio of trends obtained for the reference sensor and sensor selected for calibration, as shown below.

$$T2T_{Gain(i)\lambda} = \frac{Trend_{reference_sensor(i)\lambda}}{Trend_{Calibration_sensor(i)\lambda}} \quad (14)$$

where $T2T_{Gain(i)\lambda}$ is an expanded T2T cross-calibration gain, $Trend_{reference_sensor(i)\lambda}$ and $Trend_{Calibration_sensor(i)\lambda}$ are TOA reflectance obtained after using an MSG filter for i^{th} day.

3.8. Uncertainty Estimation Using Monte Carlo Simulation

After obtaining trend gain, uncertainty analysis was performed using Monte Carlo Simulation. The uncertainty analysis of the expanded T2T cross-calibration technique was calculated by accounting for the Uncertainty associated with data processing and random variability present in the dataset. The primary sources of uncertainty estimation accounted for sensors and site variability, SBAF, and BRDF uncertainty. This section presents the process applied for calculating the uncertainty associated with each source.

Temporal uncertainty (U_{Temporal}) was estimated considering the temporal drift and variability of the sensor and site, respectively. For each reference sensor, the standard deviation of the mean TOA reflectance for each image from each path/row was estimated, and the temporal uncertainty was calculated as the mean of the standard deviation. In contrast to the standard PICS, where each observation is made over the exact same target, EPICS Global is the combination of multiple locations throughout the world for every day of the Landsat cycle, allowing for the imaging of a different portion of the cluster. Spatial uncertainty (U_{Spatial}) taken into consideration in order to take potential variation between sites (aspects of the cluster) into account. Spatial uncertainty was calculated by accounting for the variability among the WRS path/row within EPICS Global or due to the non-uniformity of the site. The temporal standard deviation of the EPICS Global was estimated, consisting of both spatial and temporal variability of the site. Spatial Uncertainty was calculated by subtracting the temporal component from the entire EPICS Global standard deviation. SBAF uncertainty (U_{SBAF}) was calculated using the standard deviation of the 2300 SBAF values obtained from the hyperspectral data of EPICS Global. BRDF uncertainty (U_{BRDF}) accounted for from the BRDF model used for normalizing the cloud-screened dataset. The root mean square error (RMSE) of the BRDF model predicting the reflectance of the model was estimated for obtaining the BRDF uncertainty. Initially, the BRDF error was calculated as the difference between the cloud-filtered TOA reflectance and TOA reflectance predicted by the model for the reference sensor. In addition, the BRDF uncertainty was calculated by calculating the RMSE of the BRDF error calculated for each observation.

$$U_{\text{Spatial}} = U_{\text{Temporal_EPICS_Global}} - U_{\text{Temporal}} \quad (15)$$

$$\text{BRDF Error} = \rho_{\text{Observed_Reflectance}} - \rho_{\text{Predicted_Reflectance}} \quad (16)$$

It might be possible that we overestimated or underestimated uncertainty if we did not account for correlation among uncertainty sources. In the first step, the correlation among each possible pair of uncertainty sources was checked to identify whether a correlation between them exists or not. Moreover, the correlation result shows a positive and negative correlation depending on bands for each possible pair of uncertainty sources. Then, Monte Carlo simulation was done after determining the correlation to eliminate the possibility of over or under estimating Uncertainty as shown in Figure 4. After calculating all four sources of uncertainties, Monte Carlo Simulation was done, accounting for these uncertainties [33]. Initially, the correlation coefficient ($\text{Correlation_Coefficient}_{xy}$), covariance (Covariance_{xy}), and standard deviation ($\text{Std_Dev}_x \times \text{Std_Dev}_y$) between every two possible pairs as shown in Figure 5 and Equation (17), four sources of Uncertainty were calculated. Here, x and y are any two pairs of uncertainty sources. Multivariate normal random numbers were estimated 1000 times to generate the 1000 random uncertainty for each source of Uncertainty, accounting for all four sources of Uncertainty and covariance among them. The reason for a 1000 iteration is further described in the Section 5. The mean of the 1000 simulation was calculated for each source of Uncertainty and, lastly, for total Uncertainty (U_{Total}) was calculated as shown in Equation (18).

$$\text{Covariance}_{xy} = \text{Correlation_Coefficient}_{xy} \times (\text{Std_Dev}_x \times \text{Std_Dev}_y) \quad (17)$$

$$U_{\text{Total}} = \sqrt{U_{\text{Temporal}}^2 + U_{\text{Spatial}}^2 + U_{\text{SBAF}}^2 + U_{\text{BRDF}}^2} \quad (18)$$

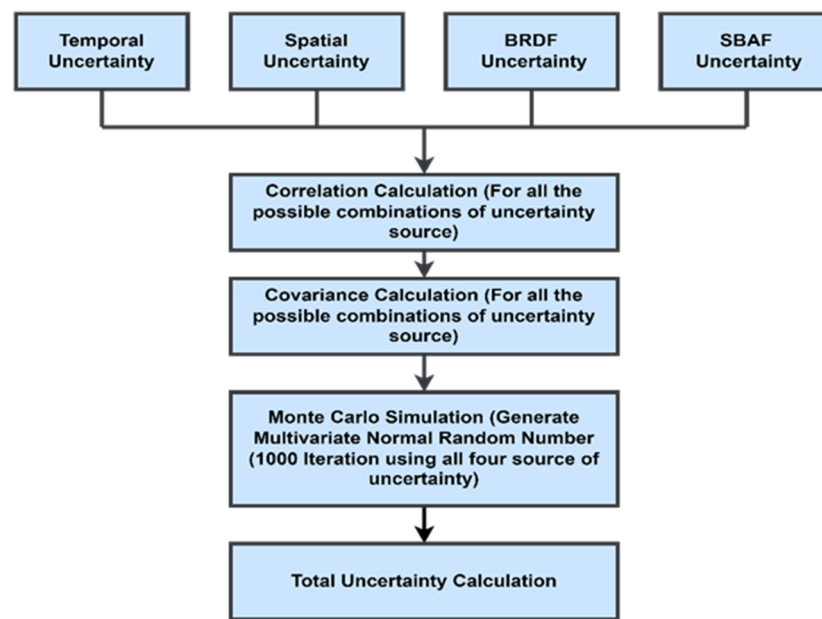


Figure 4. Flowchart showing total uncertainty estimation process after considering correlation among the source of Uncertainty and performing Monte Carlo Simulation for 1000 iterations.

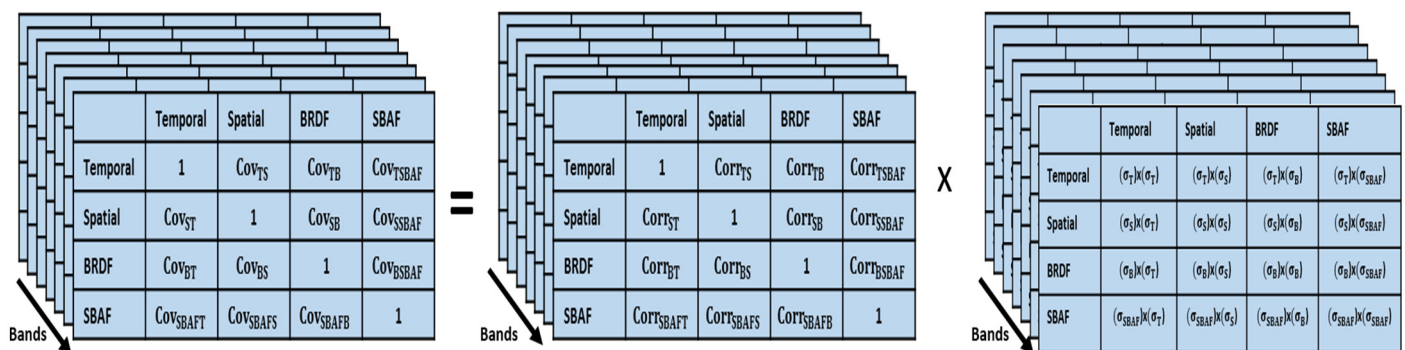


Figure 5. Block diagram-showing matrix of covariance, correlation, and standard deviation between all possible pairs of the source of Uncertainty.

4. Validation of Expanded T2T Cross-Calibration Method

After the development of the expanded T2T cross-calibration technique, the results obtained from this technique were validated with the other trusted cross-calibration technique. This validation helped in getting a sense of the accuracy of the newly developed T2T cross-calibration technique.

4.1. Expanded T2T Technique Validation Using Landsat 8 and Sentinel 2A

The expanded T2T cross-calibration technique can be validated via comparison to multiple trusted cross-calibration techniques to validate its results. For this purpose, an expanded T2T technique was applied to cross-calibrate Sentinel 2A and Landsat 8; the result was compared with multiple independent cross-calibration techniques, namely RadCaTS (Radiometric Calibration Test Sites) RRV (Railroad Valley), DIMITRI (Database for Imaging Multi-Spectral Instruments and Tools for Radiometric Intercomparison)-PICS, and SDSU APICS (Absolute PICS) Models, used by Barsi et al. [23]. This section compares the expanded T2T cross-calibration technique with these models.

An automated method for traditional ground-based vicarious radiometric calibration has been designed and developed by the remote sensing group (RSG) of the College of Optical Sciences at the UAz. In order to collect appropriate data for ground-based vicarious

calibration without onsite employees, the RadCaTS was established in RRV, Nevada [34]. The DIMITRI-PICS desert absolute calibration model simulates the TOA reflectance over predefined desert sites in the VNIR spectral range. This model has databases for image multispectral instrument tools consisting of databases and software containing geometrically and radiometrically corrected products for radiometric inter-comparison from 2002 until the present [35]. SDSU APICS model predicted TOA reflectance using PICS regions and calibrated Landsat 8 and Sentinel 2A using the traditional cross-calibration method [36].

Barsi validated the absolute calibration of OLI and MSI sensors through these models, which predict the TOA reflectance depending on sources external to the sensors. The APICS and RadCaTS RRV absolute calibration models work for all seven spectral bands, whereas the DIMITRI-PICS models only function for VNIR bands. The cross-calibration result for both sensors using DIMITRI-PICS was within 2% for all the spectral bands. Additionally, RadCaTS RRV results were within 4% for all spectral bands. APICS model indicated that both sensors were calibrated well within 0.5% except for red and CA bands.

Figure 6 demonstrates the Sentinel 2A and Landsat 8 ratio differences for these models, and error bars indicate uncertainty computed from each method. However, the author originally used the error bar as the uncertainty calculated as the standard deviation of the mean. In this figure, the expanded T2T cross-calibration result has been added as the Sentinel 2A, and Landsat 8 mean ratio and error bar represent uncertainty computed from Monte Carlo Simulation. In order to perform a fair comparison among these models, the T2T cross-calibration technique also used two years of the dataset (2015–2017) for both sensors as originally used by Barsi. The expanded T2T cross-calibration results for Landsat 8 versus Sentinel 2A show agreement with these RadCaTS RRV, DIMITRI-PICS, and APICS models with less than 1% difference on average over all the spectral bands. This result strongly supports that the expanded T2T approach shows significant agreement with the other three independent methodologies.

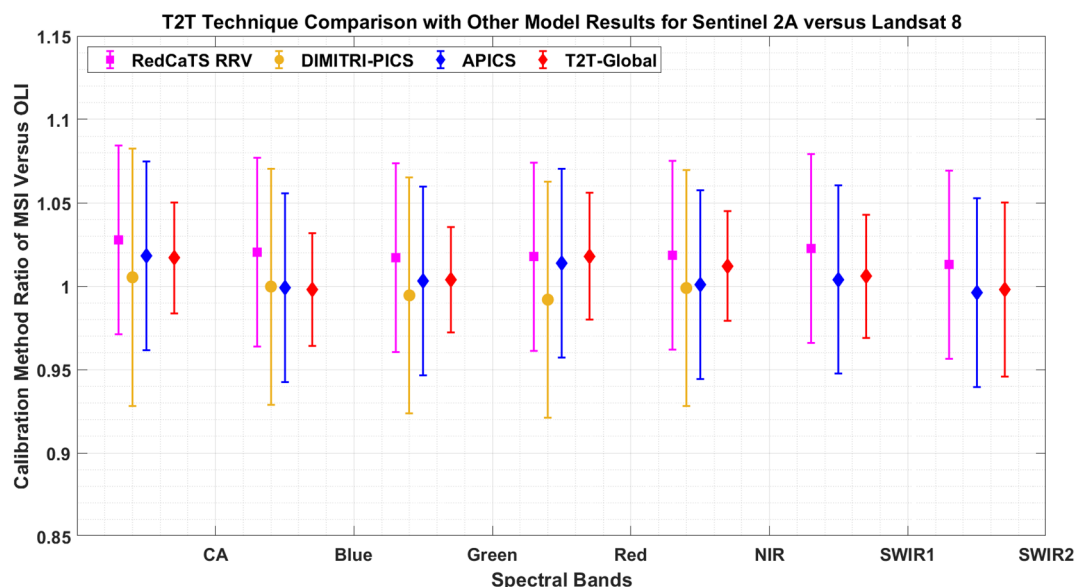


Figure 6. Trend-to-Trend Cross-Calibration result comparison with absolute calibration results for Sentinel 2A versus Landsat 8 and error bars for all models representing uncertainty. Two years of the dataset (2015–2017) for both sensors as initially used by Barsi.

4.2. SDSU Inter-Comparison for Landsat 8 and Landsat 9

The primary goal of this section is also to validate the performance of the expanded T2T cross-calibration technique, and in this case, the cross-calibration of Landsat 8 and Landsat 9 was done. SDSU Image Processing Laboratory member of the Landsat Calibration and Validation team provided multiple techniques for performance analysis of Landsat 9 compared to Landsat 8. Multiple Techniques used by SDSU for Landsat 8 and Landsat 9

cross-calibration are Underfly Events [16], Traditional EPICS Cross-Calibration [12], ExPAC Double Ratio [12], and expanded T2T Cross-calibration technique.

The expanded T2T cross-calibration technique was applied to calibrate Landsat 8 and Landsat 9 during five months of Landsat 9 in orbit using both EPICS North Africa and EPICS Global. The obtained result from this technique was compared with other SDSU calibration techniques. Figure 7 shows that the results obtained from these models agree well within a 0.5% difference on average for all spectral bands, illustrating that EPICS cross-calibration techniques are successful and comparable. The error bar on this mean represents the uncertainty associated with the independent SDSU models. The Traditional cross-calibration method and T2T technique used EPICS Global sites, whereas Calibration, ExPAC Double Ratio, also used EPICS North Africa sites. All these techniques were applied to see the satellite's performance from its first week in orbit. EPICS Global enhanced our ability to calibrate sensors by allowing us to collect multiple observations per day with global coverage.

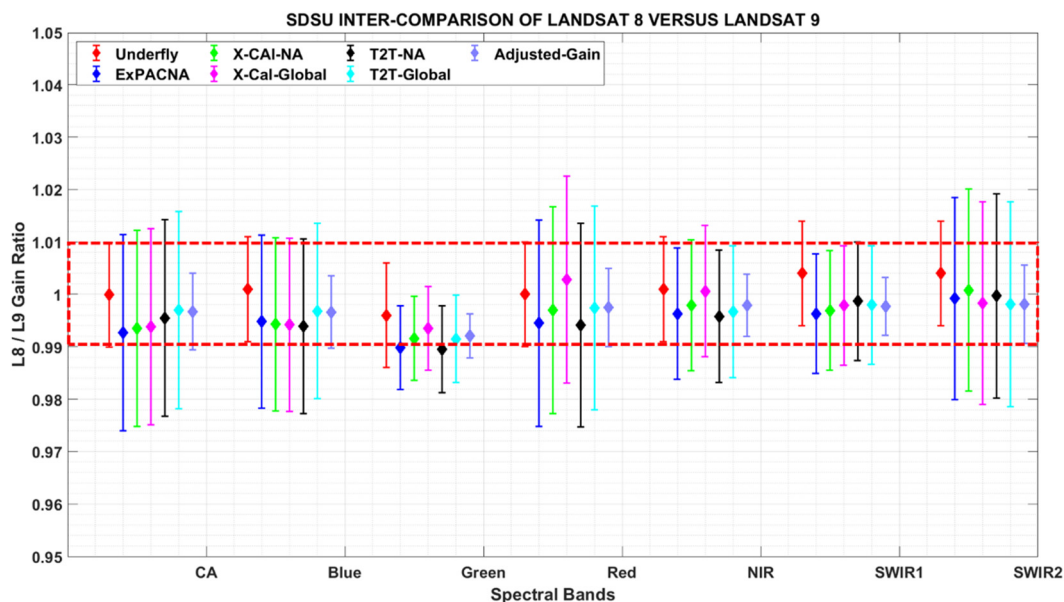


Figure 7. SDSU Inter-Comparison of Landsat 8 versus Landsat 9 results using four different techniques, and the red dotted box represents a 1% difference level.

Table 2 presents the mean gain obtained from four SDSU-independent cross-calibration techniques used for Landsat 8 and 9. The gain table shows that these methods have similar results for the calibration of these sensors. The calibration results demonstrated that the difference among these models, on average, is less than 0.5% difference within their uncertainty. With independent SDSU techniques, the difference between these sensors agrees with each other. This result supports that the T2T technique also has had potential to generate the same results as other techniques within their uncertainty.

4.3. Expanded T2T Technique Validation Using ETM+ and Terra MODIS

The primary motive of this section is also to evaluate the expanded T2T technique by cross-calibrating Terra MODIS and ETM+ and validate the results with the technique presented by Amit et al. [37]. The author used four PICS sites to assess the calibration difference between these two sensors in their reflective bands. Initially acquired, the scenes from these sensors, were corrected for bidirectional reflectance, adjusted spectral response function mismatch, and incorporated atmospheric water-vapor impacts to provide the long stability of both instruments. The author shows the long-term stability among these two sensors from 2000 to 2017 was within 2%.

Table 2. Cross-calibration gain for Landsat 8 and Landsat 9 using different techniques used by SDSU Image Processing Laboratory.

Xcal Ratio	CA	Blue	Green	Red	NIR	SWIR1	SWIR2
Underfly	1.0010	1.0020	0.9960	1.0000	1.0010	1.0030	1.0040
ExPAC-NA	0.9927	0.9948	0.9898	0.9945	0.9963	0.9963	0.9992
XCal-NA	0.9935	0.9943	0.9916	0.997	0.9979	0.9969	1.0008
XCal-Global	0.9938	0.9942	0.9935	1.0028	1.0006	0.9979	0.9983
T2T-NA	0.9955	0.9939	0.9895	0.9941	0.9958	0.9987	0.9937
T2T-Global	0.9970	0.9968	0.9915	0.9974	0.9967	0.9980	0.9951
Adjusted Gain	0.9967	0.9966	0.9921	0.9975	0.9979	0.9977	0.9981

In order to compare the expanded T2T cross-calibration technique, both sensors were cross-calibrated for the same time period for a fair comparison. EPICS global sites were used to determine the difference between these sensors. After obtaining the difference between Terra MODIS and ETM+, differences were plotted with the result obtained by Amit to evaluate the performance of the expanded T2T technique. Angal presented that the larger disagreement of these sensors was 5% for the shortest wavelengths and other wavelengths are within $\pm 2\%$.

Figure 8 shows the difference among sensors using both methods for all four sites, namely Libya 4, Libya 1, Niger 1, and Niger 2, and results from EPICS global using expanded T2T cross-calibration technique. Blue dots represent the sensor's difference obtained from the expanded T2T technique, whereas magenta dots represent the difference obtained from the author's technique for four PICS sites at different wavelengths. The results demonstrate that these two models show agreement within a 1% difference on average over all the spectral bands and sites. Generally, NIR 0.86 μm is impacted by both vegetation and water vapor. The Niger locations have more water vapor compared to the Libya sites. Here, visible channels and the SWIR1 channel are not impacted by the water vapor and show good agreement. Since the EPM+ NIR band is much broader, it includes water vapor absorption and the window. Therefore, for this channel accounting for water vapor is crucial. At some wavelengths, the expanded T2T approach shows a difference with these sites, and it may be because EPICS Global includes 33 sites, and four individual sites are in the graph. However, EPICS global also includes these four PICS in its classification. Additionally, T2T results used EPICS Global with 33 sites, and the results still match with all the four individual PICS sites used for the analysis. Hence, it can be concluded that the expanded T2T approach gives comparable and successful results.

The described technique gives mean cross-calibration gain for the sensor pairs; however, the expanded T2T technique gives a cross-calibration trend gain on a daily basis, as described in the Section 3. The daily trend gain can be used for analyzing the performance of the sensors through further analysis of the short-term and long-term trends. The daily assessment substantially increases the sample size and therefore reduces estimating degradation over a longer period.

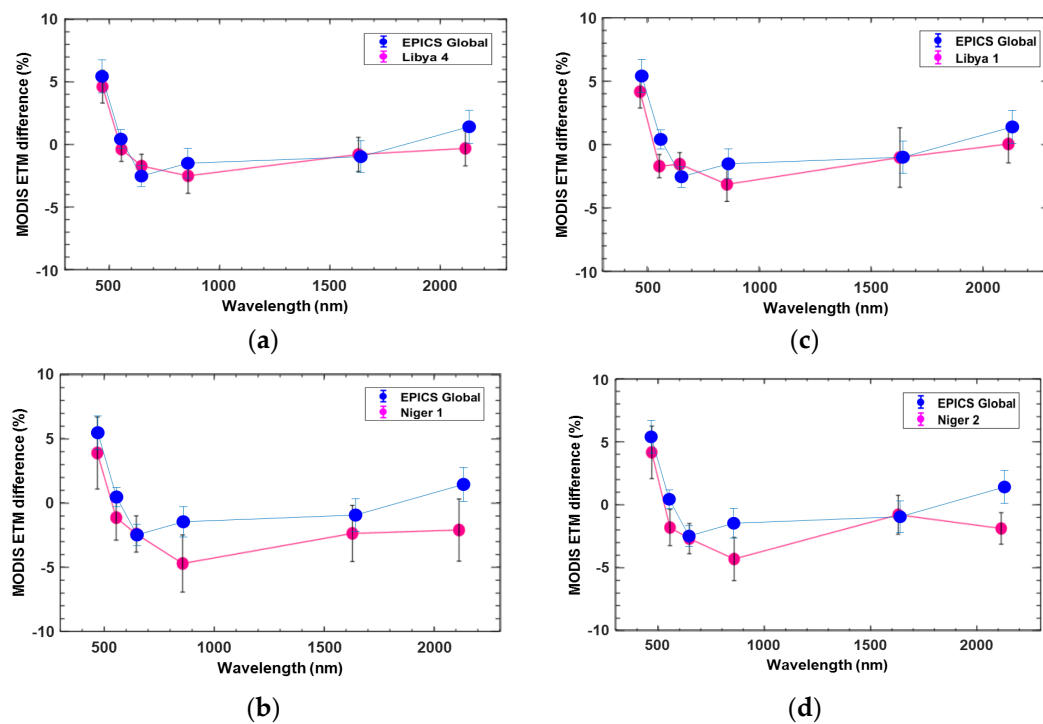


Figure 8. Terra MODIS and ETM+ difference, blue and magenta dots are for T2T and Amit’s methods, respectively, for all solar bands. (a–d) are Libya 4, Niger 1, Libya 1, and Niger 2 sites and plotted EPICS Global results with all 4 PICS sites.

5. Results and Discussion

5.1. Expanded T2T Cross-Calibration Application

After validating the expanded T2T cross-calibration technique with other trusted techniques, it is clear that this model shows significant agreement with other cross-calibration models. After that, the expanded T2T cross-calibration technique was applied to the global scale by using EPICS global as a site. Additionally, the comparison between EPICS Global and North Africa is shown in this section using the expanded T2T technique to show model performance when expanded to a global scale.

5.1.1. Stepwise Results for Global Application

The stepwise result sections will present results obtained from each step involved in the expanded T2T cross-calibration technique. This section demonstrated the results for one pair of cross-calibration such that Landsat 8 and Terra MODIS as reference sensors and sensors selected for calibration. This section provided insight into the overall mechanism of the expanded T2T cross-calibration technique.

Global SBAF Estimation

Initially, the observations for both Landsat 8 and Terra MODIS were acquired, and after that, these scenes were cloud filtered. Then, SBAF values were computed to match the response of the reference sensor and the sensor selected for calibration. The Hyperion satellite was used to obtain a hyperspectral measurement of the EPICS Global sites. The hyperspectral profile for EPICS global was estimated by using 2300 images from 57 paths/rows, capturing the information of all the pixels of the EPICS global cluster. Figure 9 shows the RSR profile of Landsat 7, Landsat 8, Landsat 9, Terra MODIS, Aqua MODIS, Sentinel-2A, and Sentinel-2B, along with the hyperspectral curve obtained from Hyperion for coastal aerosol, blue, green, red, NIR, SWIR1, and SWIR2 channels. RSR of Landsat 8 is very similar to Landsat 9 for corresponding bands because they have the same spectral characteristics. Likewise, the RSR of Sentinel-2A and Sentinel-2B and the RSR

of Aqua MODIS and Terra MODIS match each other because these pairs of satellites also have similar spectral characters and are from the same family. The black Hyperion line represents the mean of the 2300 images obtained while estimating the hyperspectral profile of the target.

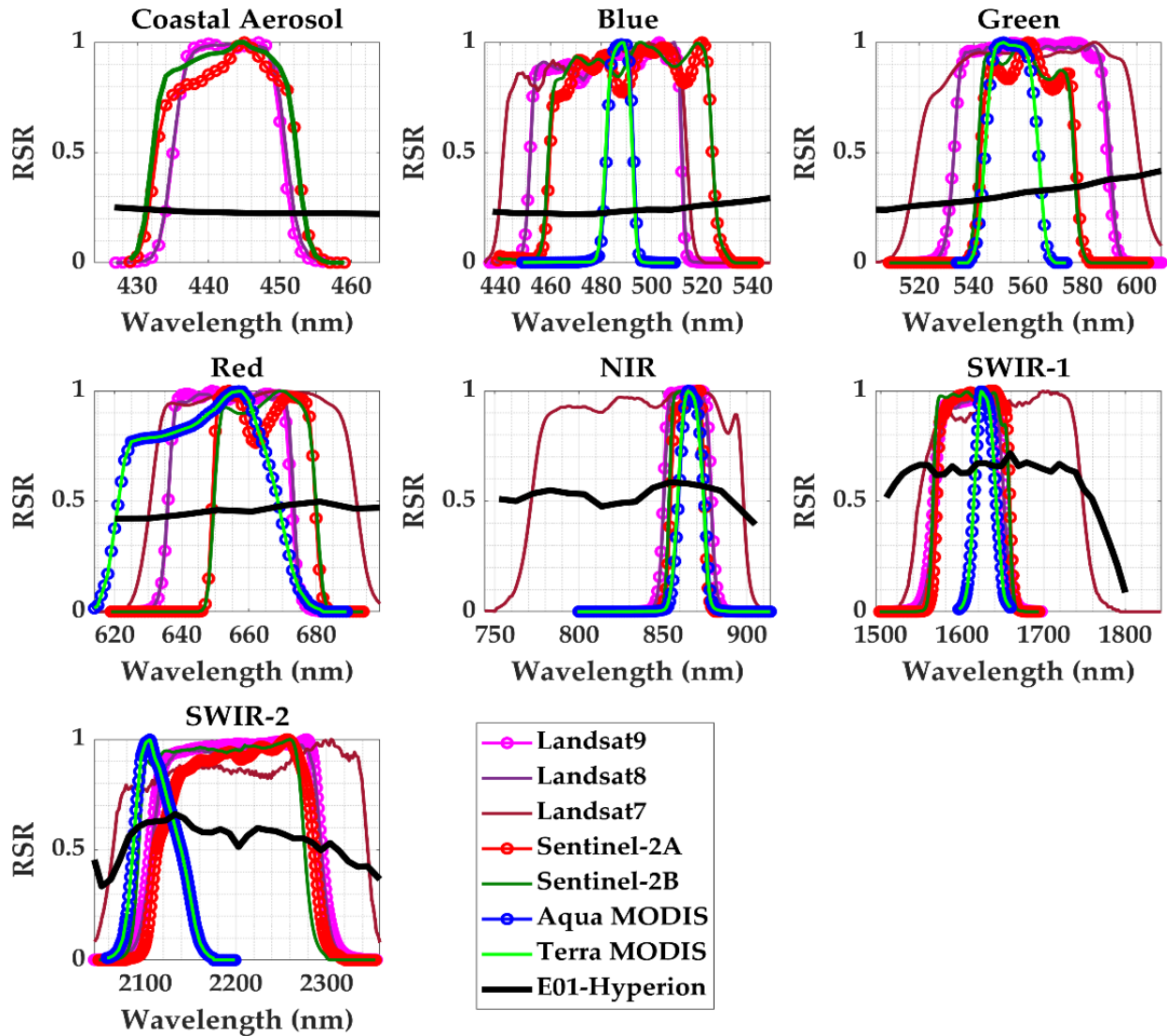


Figure 9. RSR of Landsat 9, Landsat 8, Landsat 7, Sentinel-2A, Sentinel-2B, Aqua MODIS, Terra MODIS, and the hyperspectral profile of Hyperion derived using EPICS Global.

Figure 10 shows the SBAF values calculated for all six sensors compared with Landsat8 for all spectral bands. In applying the expanded T2T technique to a global scale, Landsat 8 was considered the reference sensor for all six pairs, and Landsat 7, Landsat 9, Aqua MODIS, Terra MODIS, Sentinel 2A, and Sentinel 2B as a sensor to be calibrated. SBAF values for Landsat 8 versus Landsat 9/Sentinel 2A/Sentinel 2B are close to unity for all the spectral bands. Whereas SBAF values for Landsat 8 versus Landsat 7/Aqua MODIS/Terra MODIS deviated from unity due to the combinations of both hyperspectral shape and RSR, as shown in Figure 9. ETM+ NIR band spectral response is wider than shorter wavelengths, and the larger width also contains more absorption features. Additionally, for the SWIR2 channel, in the beginning, the spectral response shows a water band absorption feature, whereas later spectral response resides in the window.

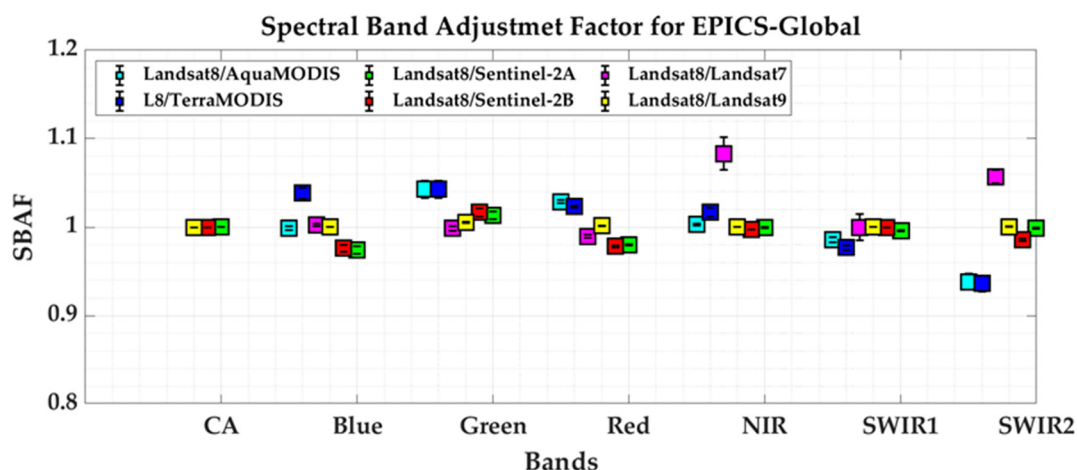


Figure 10. SBAF values calculated from the hyperspectral profile of Hyperion derived using Global EPICS for six pairs of sensors combination where Landsat 8 is as reference sensor, and denominator sensors are sensors needed to be calibrated. Error bars are the standard deviation ($k = 2$).

Figure 11 demonstrates the application of the SBAF values to Terra MODIS for the SWIR 2 band. Here, black and blue dots represent cloud-filtered TOA reflectance for Landsat 8 and Cloud filter Terra MODIS. Additional red dots represent SBAF applied TOA reflectance for Terra MODIS for the SWIR2 band using EPICS Global. The red line shows the mean of the SBAF-applied TOA reflectance for Terra MODIS, which demonstrated that after the application of the SBAF, the mean line of cloud-filtered Terra MODIS shifted close to Landsat 8. This result shows that SBAF helped adjust the two sensors' spectral response. There are large seasonal cycles, and daily noise can be seen because of the water vapor variability.

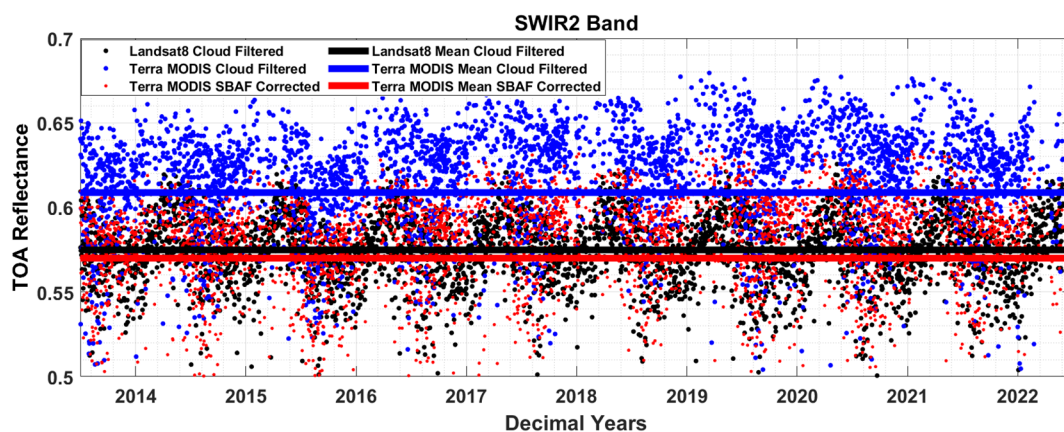


Figure 11. Black, blue and red dots represent cloud-filtered Landsat 8, Cloud filter Terra MODIS, and SBAF corrected Terra MODIS TOA reflectance for SWIR2 band using EPICS Global.

Cloud-Filtered and BRDF Normalized TOA Reflectance

After SBAF adjustment, both datasets were BRDF normalized. A single BRDF model was applied to predict the reflectance of all sensors to normalize them to a common reference angle, as the directional effect is concerned with the target. A standard set of reference angles for solar zenith and azimuth and sensor zenith and azimuth angles were selected and applied to all sensors to scale their reflectance to the same level. Hence, 130° solar azimuth, 30° solar zenith, 105° view azimuth, and 3° view zenith angle were selected as common reference angles for BRDF normalization. The solar and view reference angles are calculated from the dataset and their polar projection. These angles were used for calculating the TOA reflectance predicted by the model.

Figure 12 shows the example of the BRDF model predicted TOA reflectance using cloud-filtered TOA reflectance of Landsat 8 for the Red channel. This example demonstrates that the model successfully predicts the cloud-filtered TOA reflectance within 0.0356% means residual error. The model could predict the nature of the target for all the sensors used in this research with a very small residual error. The BRDF normalized TOA reflectance of the Landsat 8 NIR band for EPICS Global was generated by scaling using the above reference angles after predicting the TOA reflectance using the 15-coefficient model. Figure 13 illustrates the improvement of the site's directional effect after applying the BRDF model to the dataset. Black dots show cloud-filtered TOA reflectance, and magenta dots show BRDF normalized TOA reflectance for Landsat 8 SWIR1 band for EPICS Global. The figure demonstrates that the seasonal oscillatory pattern of Landsat 8 cloud-filtered TOA reflectance was substantially reduced using BRDF Model.

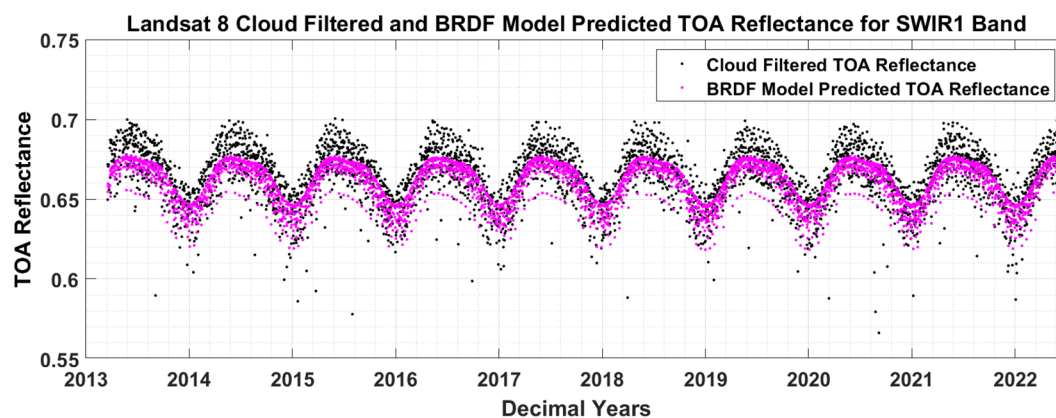


Figure 12. Black and magenta dots represent cloud-filtered TOA reflectance, and the BRDF model predicted the TOA reflectance of Landsat 8 for the SWIR1 Band.

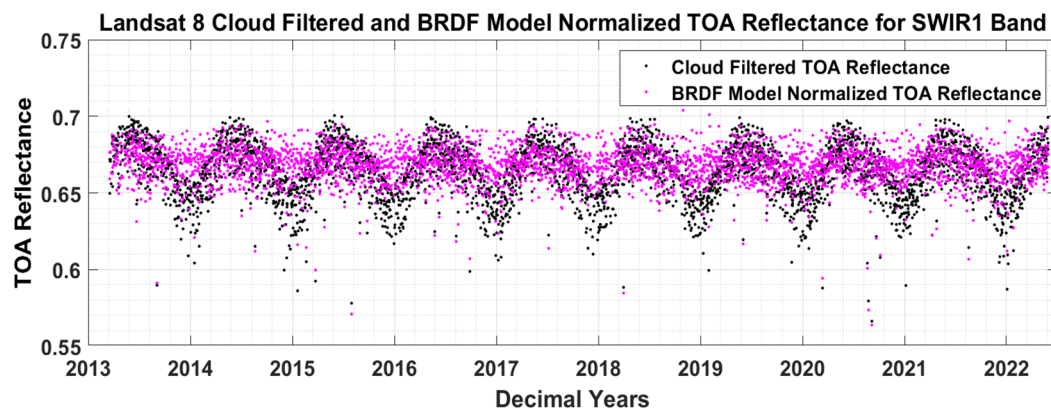


Figure 13. Black and magenta dots represent cloud-filtered TOA reflectance and BRDF normalized TOA reflectance of Landsat 8 for SWIR1 Band.

Trend Identification Using MSG Filter

MSG smoothing was done for both sensors after BRDF normalization. The expanded T2T cross-calibration technique used a 120-day window size. Figure 14 represents the MSG filtered TOA reflectance trend for a red band of Landsat 8 with 60 and 120-day window sizes. We expect a continuous and smooth function of the satellite sensor's response unless something real happens to the satellite that would cause an abrupt change. There is a discontinuity in the trend obtained by the 60-day window size, as seen in the figure. Additionally, the magenta line has sharp terminal points, which do not seem to be real. We do not expect sharp terminal peak features and discontinuity in the dataset. Therefore, to overcome these sharp features and discontinuity window size was increased

to 120 days. The blue trend line with a 120 days window size shows the continuous and smooth function of the dataset. Additionally, it helped in dampening the sharp terminal peak features compared to the 60-day window size. Additionally, during some periods of time year, cloud cover increases, and the frequency of data collected can be impacted; the larger windows also reduced the impact of these windows while still allowing for the detection of shorter-term changes.

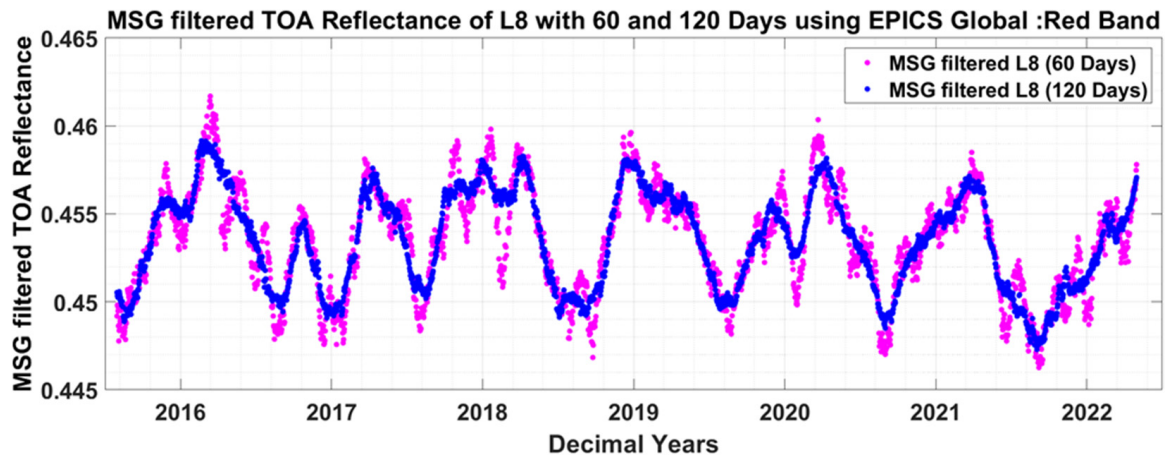


Figure 14. Magenta and blue dots represent MSG filtered TOA reflectance trend with 60 days and 120 days window sizes, respectively.

Figures 15 and 16 demonstrate the MSG smoothed trend line for Landsat 8 and Terra MODIS for the red band represented by a magenta line and black dots represent BRDF normalized TOA reflectance. The magenta line is the trended line obtained through MSG smoothing and interpolation. The detected trend line for both sensors follows their BRDF normalized data set represented by black dots. The trended line shows the original trend of the dataset, and some of the outliers were filtered with 120 days window size and 3rd-order polynomial.

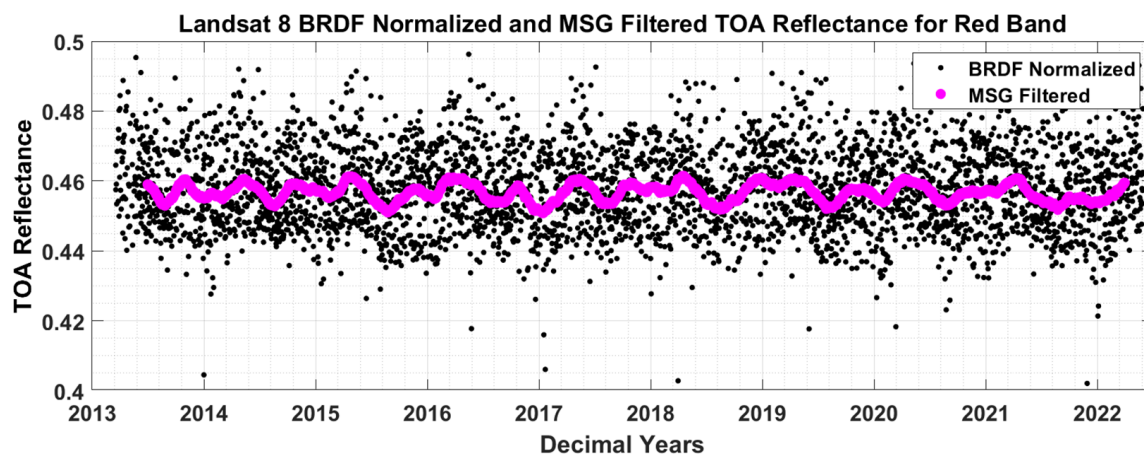


Figure 15. Black and magenta dots represent BRDF normalized TOA reflectance, and MSG filtered TOA reflectance of Landsat 8 for Red Band.

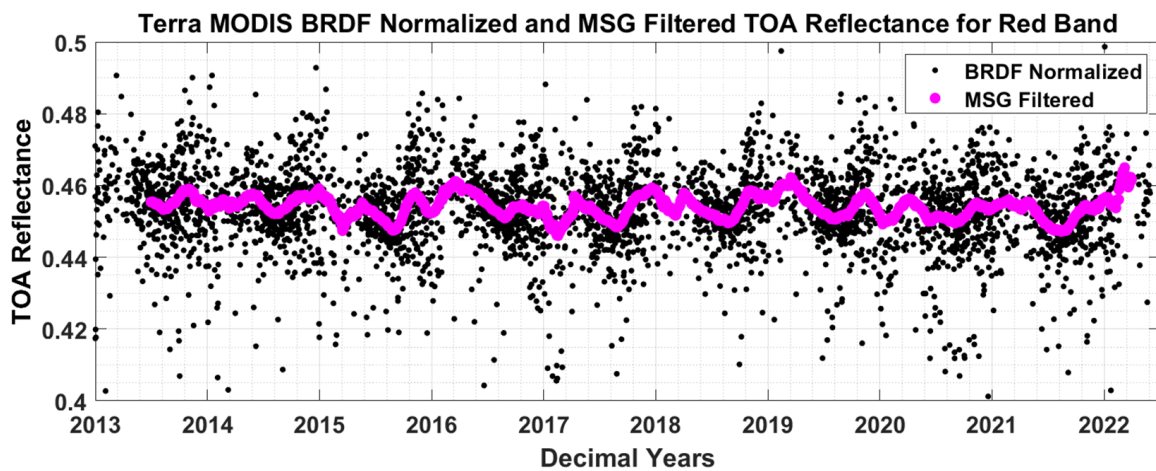


Figure 16. Black and magenta dots represent BRDF normalized TOA reflectance, and MSG filtered TOA reflectance of Terra MODIS for Red Band.

T2T Gain and Uncertainty Using Monte Carlo Simulation for Single Pair

Uncertainty for all pairs of sensor calibration was estimated according to the steps described in the Section 3. Figure 17 represents the total uncertainty estimated for Landsat 8 versus Terra MODIS using a different number of iterations to illustrate the reason for selecting a significant number of iterations for Simulation. We can see from the graph that 10, 50, and 100 iteration uncertainties have not converged for all the bands and that it starts converging with an increasing number of iterations. After 1000 iteration, uncertainty is stable; for this analysis, therefore 1000 iteration was selected and used for all pairs of sensors comparison.

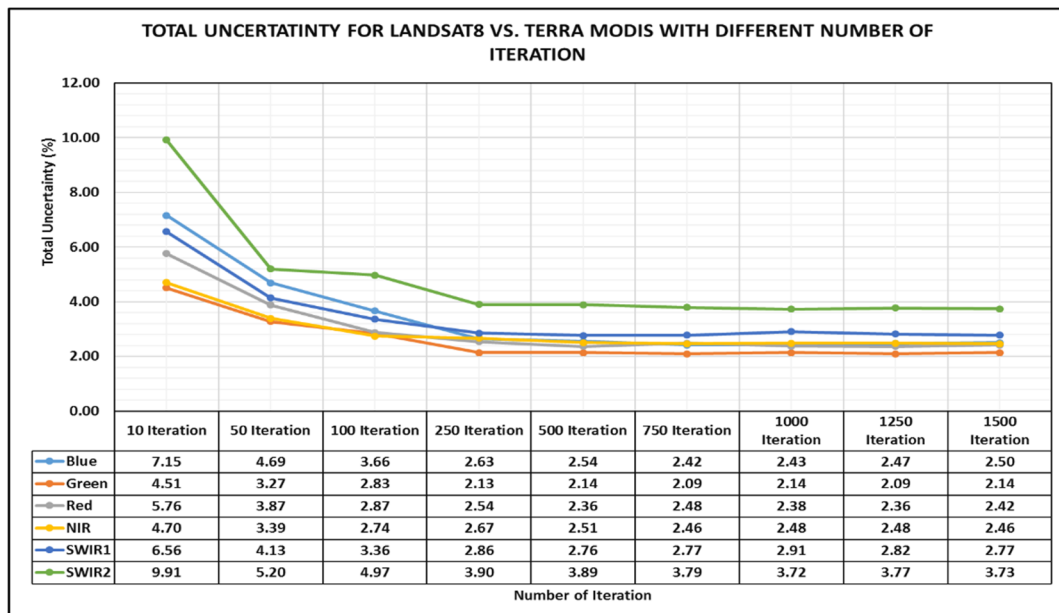


Figure 17. Total Uncertainty for Landsat 8 versus Terra MODIS with different numbers of iterations for all six bands using EPCIS Global.

After obtaining the trend of each pair of sensors using the MSG smoothing, trend-to-trend cross-calibration gain was obtained by taking the ratio reference sensor over the sensor selected for calibration. The cross-calibration trend obtained from the sensor pairs on daily assessments can be used for analyzing the sensor performance. The sensor performance can be determined by analyzing the sudden step change in the trend. Figure 18 indicates the trended gain between Landsat 8 and Terra MODIS for six bands, along with

the mean gain in the black dotted line and the uncertainty shade. The mean difference between Landsat 8 and Terra MODIS is within 4% for blue and green bands, 1% for red and NIR bands, 2% for the SWIR1 band, and 3% for the SWIR2 band. The gain Plot for SWIR1 and SWIR2 bands shows that after 2016, the magnitude of the trend increased significantly because Terra MODIS experienced a safe mode anomaly in February 2016, during which this instrument also transitioned to safe mode [38].

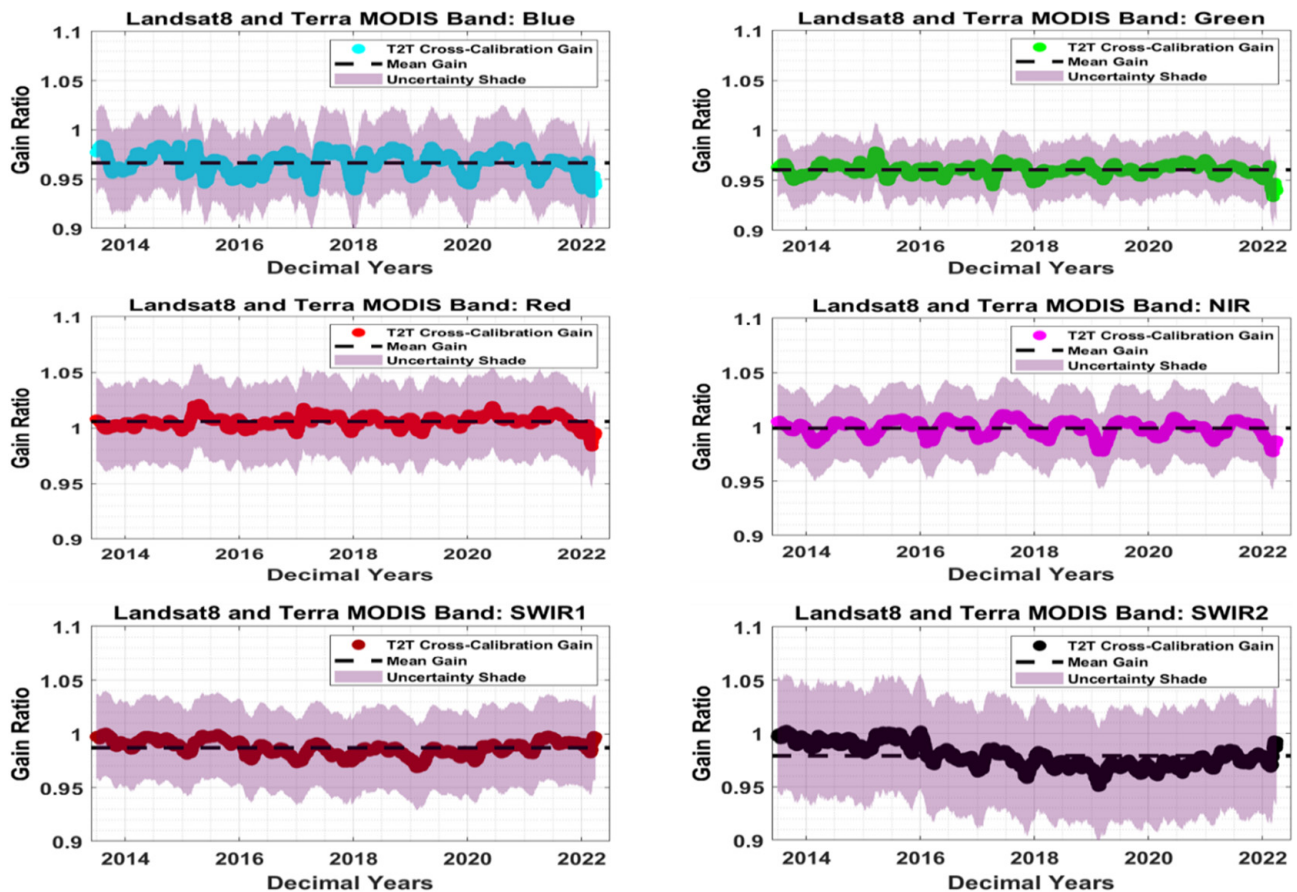


Figure 18. Trend-to-Trend Cross Calibration Gain with Mean Gain and Shaded region shows uncertainty associated with specific bands.

The shaded region on each band shows uncertainty associated with them. As mentioned in the Section 3, four sources of uncertainty were considered, correlation among these sources was determined, and Monte Carlo Simulation was applied with 1000 iterations. Table 3 shows uncertainty sources and total uncertainty for Landsat 8 vs. Terra MODIS for EPICS Global using Monte Carlo Simulation. After accounting for correlation, BRDF uncertainty was within 0.3% percent for each band for this pair of sensors. Likewise, temporal and spatial uncertainty and SBAF were within 1.5–3% for Landsat 8 vs. Terra MODIS. In addition, Total Uncertainty was within 3% for all bands except for the SWIR2 band, which was 3.8%. In addition, the calibration uncertainty for Landsat 8 is 2% for all the bands.

5.1.2. Combined T2T Cross-Calibration Result Using EPICS Global

Combined plots include band-wise expanded T2T cross-calibration gain for Landsat 8 versus Landsat 7, Landsat 9, Terra MODIS, Aqua MODIS, Sentinel-2A, and Sentinel-2B, along with mean gain and uncertainty shades for each pair. Figure 19 presents Landsat 8 versus sentinel 2A/2B and Landsat 9 trend gain, mean gain, and uncertainty shade. Trend gain result in all three pairs of cross-calibration shows good agreement with a mean gain

difference of less than 1%. Sentinel 2A/2B and Landsat 9 follow each other when compared to Landsat 8, with total uncertainty within 3.5%.

Table 3. T2T Cross-Calibration Uncertainty for Landsat 8 versus Terra MODIS using Monte Carlo Simulation.

Uncertainty Source (%)	Bands					
	Blue	Green	Red	NIR	SWIR1	SWIR2
Landsat 8 Calibration	2	2	2	2	2	2
Temporal	2.00	1.53	1.64	1.23	1.31	2.86
Spatial	1.56	1.64	1.84	2.09	2.55	2.67
SBAF	1.87	1.41	1.61	1.25	1.36	2.66
BRDF	0.29	0.27	0.28	0.29	0.27	0.26
Total	2.52	2.09	2.45	2.38	2.89	3.77

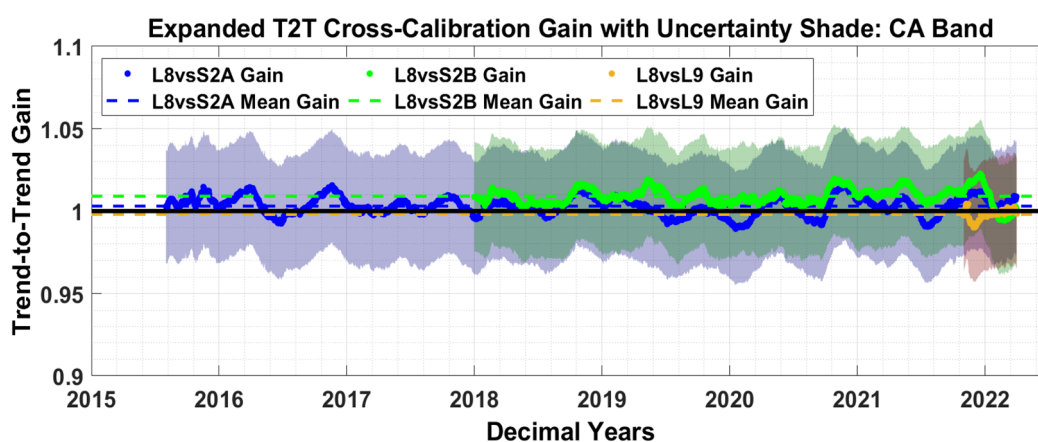


Figure 19. Expanded T2T cross-calibration gain of Landsat 8 versus Sentinel-2A/2B and Landsat 9 for coastal aerosol Band using EPICS Global. The shaded region shows uncertainty associated with each pair of sensors.

Figures 20–25 shows the Expanded T2T Cross-Calibration Gain of Landsat 8 versus Terra/Aqua MODIS, Sentinel-2A/2B, Landsat 7, and Landsat 9 for all spectral bands using EPICS Global. Except for Landsat 8 versus Terra and Aqua MODIS for the blue and green bands, the expanded cross-calibration gain is centered on one for all sensor pairs comparison for all the bands. Figure 19 shows some sensors, there are seasonal variations, and for other pairs, the T2T cross-calibration gain trends are flat. The yearly oscillation in the trend of Landsat 8 versus Aqua and Terra MODIS was predominantly caused because of the atmospheric BRDF effect and surface. It is more evident for Aqua and Terra MODIS, whereas it's less impacted for other sensors. Landsat 9, Sentinel 2A and Sentinel 2B were considered highly calibrated sensors, and their cross-calibration with Landsat 8 and, with this technique, their difference is within 1% for all the spectral bands. Additionally, the expanded cross-calibration for Landsat 8 versus Aqua and Terra MODIS is within 2.5% for all the spectral bands except for the blue band, which is within a 5% difference. Similarly, Landsat 8 and Landsat 7 expanded T2T gain difference is within 2.5 for all the spectral bands. However, the overall difference among these pairs of cross-calibrations is, on average less than 1% over all the bands. The Expanded T2T technique helps in obtaining the calibration trend of the sensor pairs on a daily assessment basis, which helps in substantially increasing the sample size. Therefore, daily assessment of trend gain reduced the uncertainty while estimating the degradation in a longer period. The expanded T2T cross-calibration technique helped in cross-calibrating the newly launched sensors as it used EPICS global sites by obtaining a dense dataset.

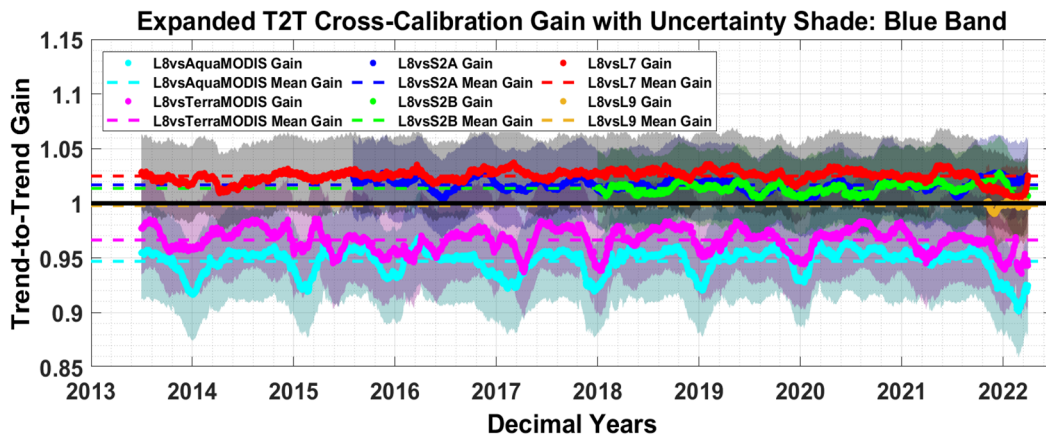


Figure 20. Expanded T2T cross-calibration gain of six sensor pairs for the blue band using EPICS Global. The shaded region shows uncertainty associated with each pair of sensors.

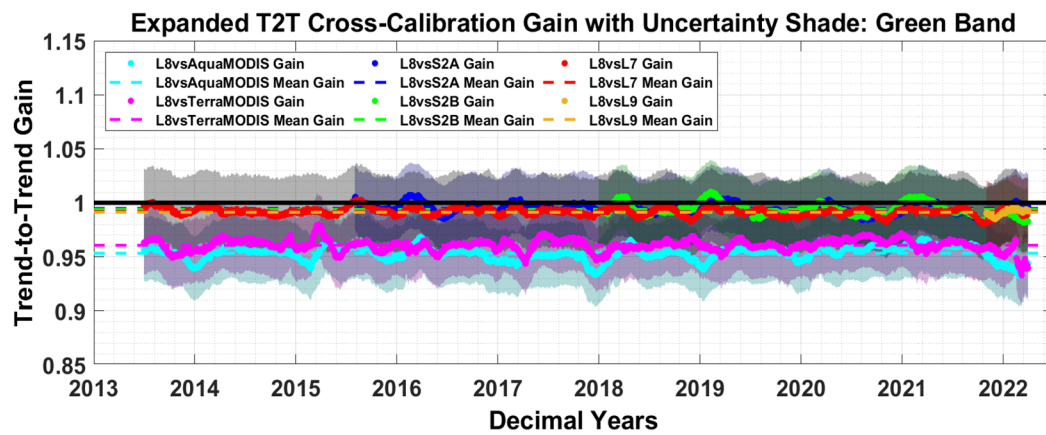


Figure 21. Expanded T2T cross-calibration gain of six sensor pairs for the green band using EPICS Global. The shaded region shows uncertainty associated with each pair of sensors.

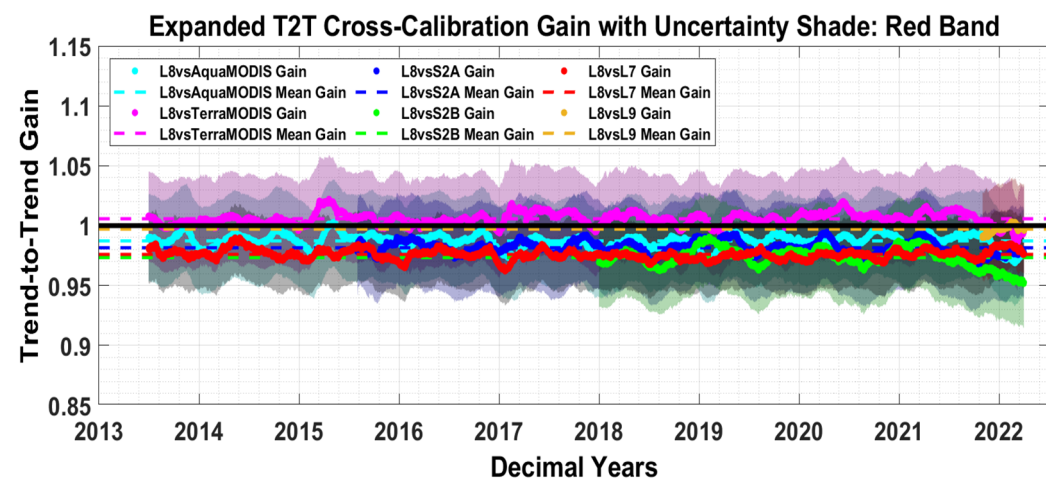


Figure 22. Expanded T2T cross-calibration gain of six sensor pairs for the red band using EPICS Global. The shaded region shows uncertainty associated with each pair of sensors.

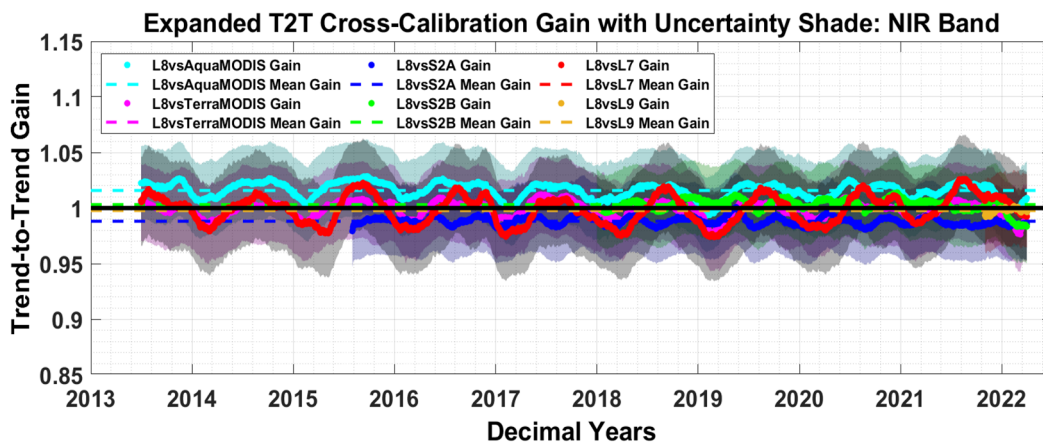


Figure 23. Expanded T2T cross-calibration gain of six sensor pairs for the NIR band using EPICS Global. The shaded region shows uncertainty associated with each pair of sensors.

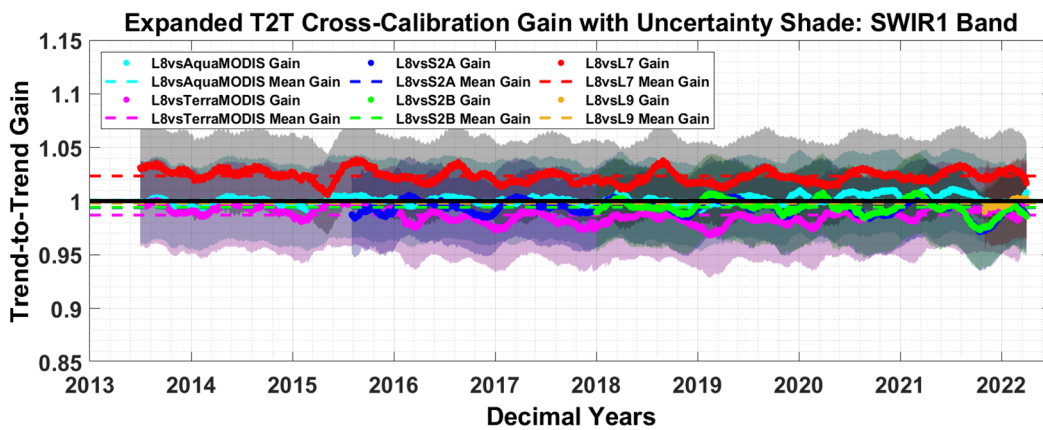


Figure 24. Expanded T2T cross-calibration gain of six sensor pairs for the SWIR1 band using EPICS Global. The shaded region shows uncertainty associated with each pair of sensors.

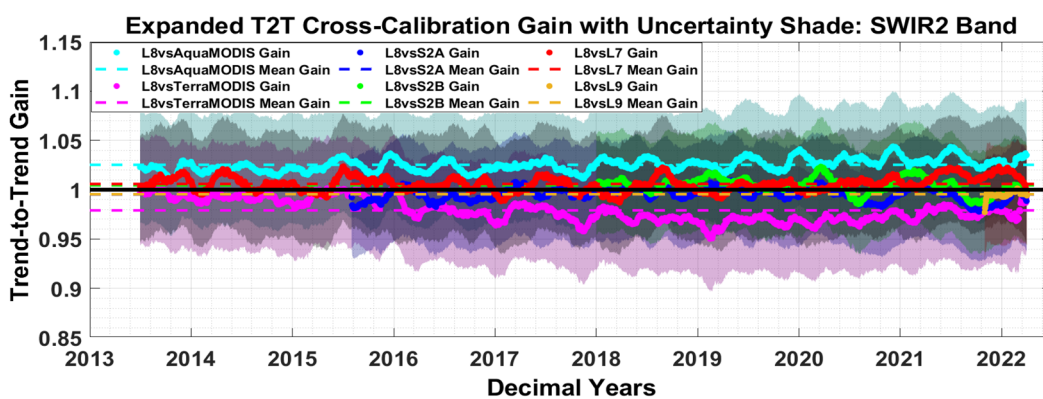


Figure 25. Expanded T2T cross-calibration gain of six sensor pairs for the SWIR2 band using EPICS Global. The shaded region shows uncertainty associated with each pair of sensors.

The shaded region in Figures 19–24 shows the total uncertainty associated with each pair of sensors comparison for that band. As mentioned above, the total uncertainty was estimated using Monte Carlo simulation considering four sources of uncertainty such that spatial, temporal, SBAF, and BRDF, and uncertainty of the reference sensor. Table 4 shows the gain and total uncertainty calculated for six sensor pairs in all the bands. The total uncertainty for the coastal aerosol band is within 3.5% for all three pairs of sensors. For all

the combinations, the total uncertainty for shorter wavelengths was within 4% for all the spectral bands except for the SWIR2 band, which is within 5%.

Table 4. Expanded T2T cross-calibration mean gain and total uncertainty for six pairs of sensors using EPICS Global.

Gain and Uncertainty	Sensors Pairs	Bands						
		CA	Blue	Green	Red	NIR	SWIR1	SWIR2
Gain	L8 vs. Aqua	—	0.9496	0.9533	0.9872	1.0158	1.0009	1.0253
Uncertainty (%)	MODIS	—	2.49	2.14	2.48	2.42	2.87	3.84
Gain	L8 vs. Terra	—	0.9664	0.9606	1.0058	0.9988	0.9870	0.9791
Uncertainty (%)	MODIS	—	2.52	2.09	0.45	2.38	2.89	3.77
Gain	L8 vs. Sentinel2A	1.0030	1.0168	0.9947	0.9815	0.9881	0.9939	0.9952
Uncertainty (%)	Sentinel2A	3.32	3.37	3.16	3.80	3.29	3.73	5.23
Gain	L8 vs. Sentinel2B	1.0091	1.0136	0.9939	0.9733	1.0031	0.9940	1.0044
Uncertainty (%)	Sentinel2B	3.41	3.39	3.08	3.74	3.30	3.68	4.99
Gain	L8 vs. L9	0.9980	0.9978	0.9912	0.9971	0.9977	0.9981	0.9954
Uncertainty (%)	L8 vs. L9	3.45	3.44	3.01	3.45	3.23	3.68	5.13
Gain	L8 vs. L7	—	1.0249	0.9919	0.9760	0.9987	1.0234	1.0058
Uncertainty (%)	L8 vs. L7	—	3.39	3.28	2.93	4.11	3.69	5.10

5.2. EPICS Global versus EPICS North Africa

The comparison between the application of the expanded T2T cross-calibration technique on EPICS Global and North Africa is explained in this section. A total number of 2712 and 3992 scenes were acquired for Landsat 8 using EPICS North Africa and EPICS Global, respectively, for the same time. EPICS Global helped to obtain a significantly dense dataset compared to EPICS North Africa at the same time. Due to this reason, EPICS Global is more efficient in calibrating newly launched sensors in a shorter time.

The expanded T2T cross-calibration gain was calculated following the steps described in the Section 3 for both EPICS Global and EPICS North Africa sites. For both, the same expanded T2T cross-calibration steps were used to make a fair comparison among them. Here, also, calibration of six pairs of sensors was performed as mentioned in the previous section. The main goal of this comparison was to evaluate the efficacy of the expanded T2T technique as it was expanded from a continent to a global scale.

After computing the cross-calibration gain for all six pairs of both sites, the ratio of trend gain was calculated for the EPICS Global and EPICS North Africa sites to see the difference among these two-cluster classifications. Figure 26 shows the expanded T2T cross-calibration gain ratio and mean gain for Terra/Aqua MODIS, Sentinel-2A/2B, Landsat 7, and Landsat 9 for EPICS Global and EPICS North Africa for the blue band, and the black dotted line shows 2.5% difference level. The average difference between these two clusters, using the expanded T2T technique, is within a 1% difference for the blue band. Likewise, Figure 27 shows the T2T cross-calibration trend gain ratio and mean gain for six pairs using EPICS Global and North Africa for the SWIR2 band. The band difference between the two sites for six sensors pair compared to Landsat 8 is within 0.5% for the SWIR2 band. This indicates that even after moving to the Global cluster with significantly more sites and more observations, the highest difference between these two sites is within 0.5–1% on average for all the bands. This gives a strong indication that the expanded T2T method works well for both sites.

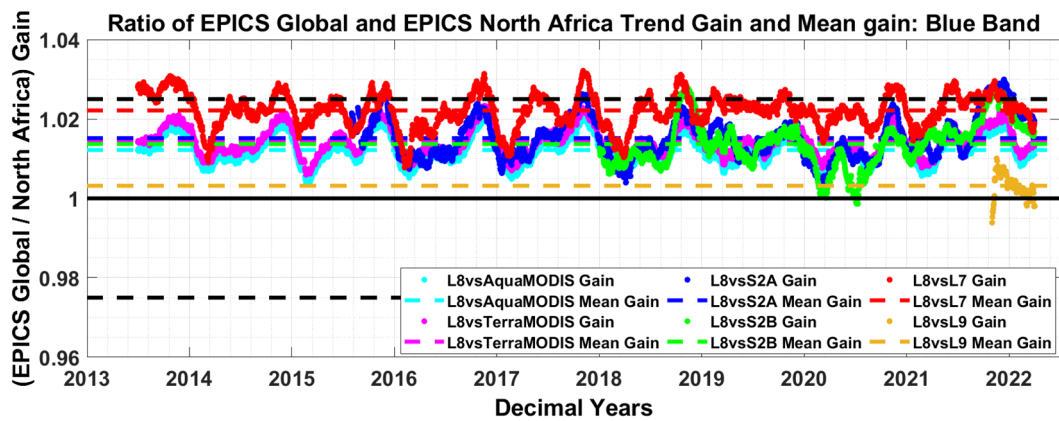


Figure 26. Ratio of EPICS Global and North Africa expanded T2T cross-calibration gain for six sensor pairs for the blue band.

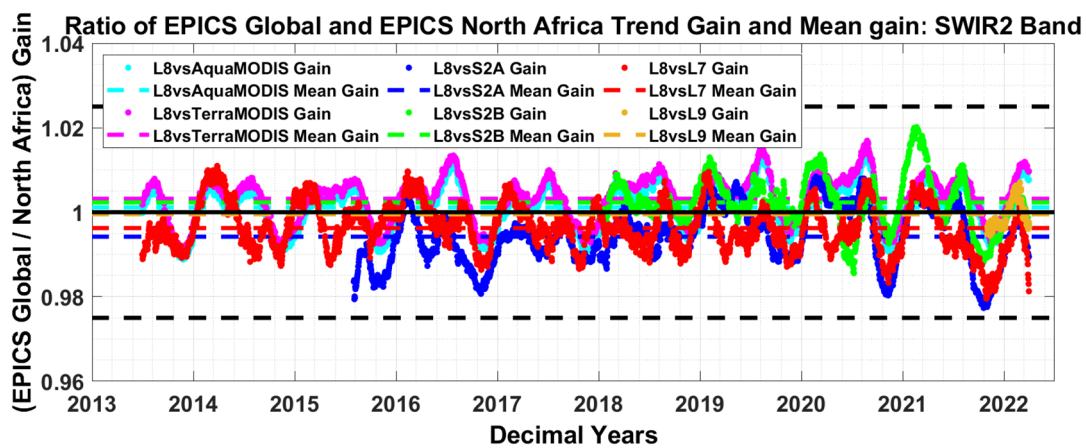


Figure 27. Ratio of EPICS Global and North Africa expanded T2T cross-calibration gain for six sensor pairs for the SWIR1 band.

Table 5 presents the ratio of cross-calibration gain for EPICS Global and North Africa using the expanded T2T technique for six sensor pairs. In this case, also, Landsat 8 was considered as the reference sensor. The table shows that the difference among sites average is within 0.5–1% difference on average for all sensor pairs and bands.

Table 5. Ratio of EPICS Global and North Africa expanded T2T cross-calibration gain for six pairs of sensors for all the bands.

The Ratio of EPICS Global and North Africa Mean Gain	Bands						
	CA	Blue	Green	Red	NIR	SWIR1	SWIR2
L8 vs. Aqua MODIS	—	1.0122	0.9936	0.9810	0.9932	1.0035	1.0011
L8 vs. Terra MODIS	—	1.0143	0.9957	0.9829	0.9952	1.0052	1.0032
L8 vs. Sentinel2A	1.0158	1.0152	0.9920	0.9802	0.9908	0.9989	0.9942
L8 vs. Sentinel2B	1.0150	1.0137	0.9937	0.9834	0.9946	1.0009	1.0023
L8 vs. L9	1.0034	1.0032	1.0012	1.0041	1.0017	0.9989	0.9995
L8 vs. L7	—	1.0221	0.9922	0.9985	1.0025	0.9945	0.9962

Table 6 shows the total uncertainty for six pairs of sensors for all bands using EPICS Global and EPICS North Africa. For both cases, total uncertainty was estimated using Monte Carlo Simulation. The total uncertainty for each pair of sensors for both EPICS Global and North Africa has statistically the same uncertainty for all the bands. Overall, the

difference in total uncertainty is less than 0.5% for all the sensor pairs in all bands for both sites. However, EPICS global sites provide comparatively dense temporal data compared to EPICS North Africa in the same time frame, at the same uncertainty level.

Table 6. Total uncertainty for all sensor pairs using Monte Carlo simulation for EPICS Global and North Africa.

Sensors Pairs	EPICS Global Total Uncertainty							EPICS North Africa Total Uncertainty						
	CA	Blue	Green	Red	NIR	SWIR1	SWIR2	CA	Blue	Green	Red	NIR	SWIR1	SWIR2
L8 vs. Aqua MODIS	—	2.49	2.14	2.48	2.42	2.87	3.84	—	2.58	2.33	3.08	2.54	3.19	3.89
L8 vs. Terra MODIS	—	2.52	2.09	2.45	2.38	2.89	3.77	—	2.67	2.32	2.96	2.56	3.28	3.80
L8 vs. Sentinel2A	3.32	3.37	3.16	3.80	3.29	3.73	5.23	3.03	3.17	2.55	3.04	2.55	3.43	4.62
L8 vs. Sentinel2B	3.41	3.39	3.08	3.74	3.30	3.68	4.99	3.10	3.09	2.58	3.03	2.63	3.34	4.74
L8 vs. L9	3.45	3.44	3.01	3.45	3.23	3.68	5.13	3.14	3.32	2.52	3.04	2.69	3.50	4.59
L8 vs. L7	—	3.39	3.28	2.93	4.11	3.69	5.10	—	3.05	3.06	2.51	3.44	2.91	4.63

6. Conclusions

The major purpose of this paper was to develop and validate the expanded T2T cross-calibration technique. The validation of the expanded T2T cross-calibration technique was done by obtaining consistent results compared to several trusted cross-calibration techniques. After validating this technique, the expanded T2T technique was applied to the global scale using EPICS global. Six sensors were calibrated with Landsat 8 as the reference sensor for this analysis. Additionally, analyzed was the difference between EPICS Global and North Africa using an expanded T2T cross-calibration technique to evaluate the performance of the model in global application. The uncertainty of the expanded T2T technique was computed using Monte Carlo Simulation. The expanded T2T technique using EPICS Global sites enhances our potential to cross-calibrate the newly launched satellite (Landsat 9) from the first week in orbit as global coverage helps to obtain 1–5 observations per day.

The expanded T2T cross-calibration technique is better compared to the T2T technique because this technique uses global sites with 33 paths/rows from North Africa, the Middle East, Central Africa, North America, and Australia, whereas the T2T technique only uses continental sites with 15 paths/rows from North Africa only. The use of the EPICS enhances the capability of the expanded T2T cross-calibration technique to calibrate the sensors monitoring the Middle East, Central Africa, North America, and Australia. The Expanded T2T technique used more sensors like Aqua/Terra MODIS to demonstrate the potential of the technique to calibrate sensors monitoring Earth for more than 20 years. The expanded T2T cross-calibration technique was also used to calibrate the newly launched satellite Landsat 9. The expanded T2T cross-calibration technique used a dense dataset with 2300 observations for hyperspectral profile estimation, which helps in better estimation of SBAF. This technique uses an MSG filter with a robust and normalized option with 120 days window size to obtain a long trend of the sensors. MSG filter with a 120 days window size helped to overcome the sharp features and discontinuity compared to a 60 days window size. Additionally, the 120 days window size reduced the impact of increased cloud coverage during some periods of time year on the dataset as a continuous and smooth function of the dataset was obtained. The expanded T2T technique has a better potential for uncertainty evaluation using Monte Carlo simulation by accounting for correlation among the source of uncertainty.

After developing the expanded T2T cross-calibration technique, it was validated by RadCaTS RRV, DIMITRI-PICS, and APICS models. The expanded T2T technique results for Sentinel2A and Landsat8 cross-calibration using EPICS global sites matched well on average within a 1% difference in their uncertainty with the other three independent

models. During Landsat 9 performance analysis compared to Landsat 8, expanded T2T cross-calibration results for Landsat 8 versus Landsat 9 using both EPICS Global and EPICS North Africa agreement within 0.5% for all the bands when compared with other SDSU IP lab techniques. Landsat 8 and Landsat 9 comparison uses five months of data from Landsat 9 in orbit. The Expanded T2T technique was also validated for Terra MODIS and ETM+ using the technique described by Amit. The expanded T2T technique using EPICS Global shows significant agreement with the model with an average difference of less than 1%. Additionally, it can be concluded that the expanded T2T cross-calibration techniques successfully agree with all the trusted models within a 1% difference level.

Furthermore, the expanded T2T technique was applied to a global scale using EPICS Global sites to evaluate the performance of the technique. Here, Landsat 8 was chosen as the reference sensor, and six sensors, namely Landsat 7, Landsat 9, Sentinel 2A/2B, and Aqua/Terra MODIS, as a sensor to be calibrated. The expanded T2T results for a global application show the overall difference among these sensor pairs, on average, is within 0.5–1% difference for all the bands. Total Uncertainty obtained for these pairs of sensors using Monte Carlo Simulation varies from 2.5% to 4% for all sensor pairs and bands except for the SWIR2 bands, which vary up to 5%. The Expanded T2T cross-calibration technique was applied to EPICS Global and North Africa sites to see their difference. The difference between these two sites was calculated using the ratio of cross-calibration gain. The ratio of EPICS Global and North Africa cross-calibration gain shows that the overall difference among these sites was, on average, within 1% difference for all the bands, as shown in Table 6. Additionally, their uncertainty also varies within 0.5% for six sensor pairs and all spectral bands. Even expanding the technique to a global scale continent, this model is within the same uncertainty level.

The expanded T2T cross-calibration technique successfully works for newly launched Landsat 9 from the first week in orbit as the technique uses EPICS Global with a temporal resolution of multiple observations per day. This technique also works well for calibrating Terra and Aqua MODIS. Even though this technique is focused on a sun-synchronous satellite's sensor, the technique could be applicable for the radiometric calibration of a geosynchronous satellite, which has the potential to image any portion of EPICS Global.

Author Contributions: Conceptualization, R.S. and L.L.; methodology, R.S. and L.L.; formal analysis R.S., L.L., M.K. and C.T.P.; supervision and funding acquisition, L.L., software, R.S. and L.L.; Validation, R.S. and M.K.; writing—original draft, R.S.; writing—review and editing; R.S. and L.L. All authors have read and agreed to the published version of the manuscript.

Funding: USGS EROS (grant number G19AS00001).

Data Availability Statement: Not applicable.

Acknowledgments: Immense thanks to Larry for his guidance and invaluable suggestions and to all the members of the Image Processing Laboratory for their continuous support and help.

Conflicts of Interest: The authors declare no conflict of interest.

References

1. Wang, D.; Morton, D.; Masek, J.; Wu, A.; Nagol, J.; Xiong, X.; Levy, R.; Vermote, E.; Wolfe, R. Impact of sensor degradation on the MODIS NDVI time series. *Remote Sens. Environ.* **2012**, *119*, 55–61. [[CrossRef](#)]
2. Barrientos, C.; Mattar, C.; Nakos, T.; Perez, W. Radiometric cross-calibration of the Chilean satellite FASat-C using RapidEye and EO-1 Hyperion data and a simultaneous nadir overpass approach. *Remote Sens.* **2016**, *8*, 612. [[CrossRef](#)]
3. Markham, B.; Barsi, J.; Kvaran, G.; Ong, L.; Kaita, E.; Biggar, S.; Czaplá-Myers, J.; Mishra, N.; Helder, D. Landsat-8 operational land imager radiometric calibration and stability. *Remote Sens.* **2014**, *6*, 12275–12308. [[CrossRef](#)]
4. Dingirard, M.; Slater, P.N. Calibration of space-multispectral imaging sensors: A review. *Remote Sens. Environ.* **1999**, *68*, 194–205. [[CrossRef](#)]
5. Thorne, K.; Markham, B.; Barker, P.S.; Biggar, S. Radiometric calibration of Landsat. *Photogramm. Eng. Remote Sens.* **1997**, *63*, 853–858.
6. Chander, G.; Mishra, N.; Helder, D.L.; Aaron, D.B.; Angal, A.; Choi, T.; Xiong, X.; Doelling, D.R. Applications of spectral band adjustment factors (SBAF) for cross-calibration. *IEEE Trans. Geosci. Remote Sens.* **2012**, *51*, 1267–1281. [[CrossRef](#)]

7. Helder, D.L.; Basnet, B.; Morstad, D.L. Optimized identification of worldwide radiometric pseudo-invariant calibration sites. *Can. J. Remote Sens.* **2010**, *36*, 527–539. [[CrossRef](#)]
8. Teillet, P.; Chander, G. Terrestrial reference standard sites for postlaunch sensor calibration. *Can. J. Remote Sens.* **2010**, *36*, 437–450. [[CrossRef](#)]
9. Bouvet, M. Radiometric comparison of multispectral imagers over a pseudo-invariant calibration site using a reference radiometric model. *Remote Sens. Environ.* **2014**, *140*, 141–154. [[CrossRef](#)]
10. Vuppula, H. *Normalization of Pseudo-Invariant Calibration Sites for Increasing the Temporal Resolution and Long-Term Trending*; South Dakota State University: Brookings, SD, USA, 2017; Available online: <https://openprairie.sdstate.edu/etd/2180/> (accessed on 15 April 2021).
11. Shrestha, M.; Hasan, M.N.; Leigh, L.; Helder, D. Extended Pseudo Invariant Calibration Sites (EPICS) for the Cross-Calibration of Optical Satellite Sensors. *Remote Sens.* **2019**, *11*, 1676. [[CrossRef](#)]
12. Shrestha, M.; Leigh, L.; Helder, D. Classification of north Africa for use as an extended pseudo invariant calibration sites (EPICS) for radiometric calibration and stability monitoring of optical satellite sensors. *Remote Sens.* **2019**, *11*, 875. [[CrossRef](#)]
13. Hasan, M.N.; Shrestha, M.; Leigh, L.; Helder, D. Evaluation of an Extended PICS (EPICS) for calibration and stability monitoring of optical satellite sensors. *Remote Sens.* **2019**, *11*, 1755. [[CrossRef](#)]
14. Khakurel, P.; Leigh, L.; Kaewmanee, M.; Pinto, C.T. Extended Pseudo Invariant Calibration Site-Based Trend-to-Trend Cross-Calibration of Optical Satellite Sensors. *Remote Sens.* **2021**, *13*, 1545. [[CrossRef](#)]
15. Fajardo Rueda, J.; Leigh, L.; Teixeira Pinto, C.; Kaewmanee, M.; Helder, D. Classification and Evaluation of Extended PICS (EPICS) on a Global Scale for Calibration and Stability Monitoring of Optical Satellite Sensors. *Remote Sens.* **2021**, *13*, 3350. [[CrossRef](#)]
16. Gross, G.; Helder, D.; Begeman, C.; Leigh, L.; Kaewmanee, M.; Shah, R. Initial Cross-Calibration of Landsat 8 and Landsat 9 Using the Simultaneous Underfly Event. *Remote Sens.* **2022**, *14*, 2418. [[CrossRef](#)]
17. Goward, S.N.; Masek, J.G.; Williams, D.L.; Irons, J.R.; Thompson, R. The Landsat 7 mission: Terrestrial research and applications for the 21st century. *Remote Sens. Environ.* **2001**, *78*, 3–12. [[CrossRef](#)]
18. Andrefouet, S.; Bindschadler, R.; Brown de Colstoun, E.; Choate, M.; Chomentowski, W.; Christopherson, J.; Doorn, B.; Hall, D.; Holifield, C.; Howard, S. *Preliminary Assessment of the Value of Landsat-7 ETM+ Data Following Scan Line Corrector Malfunction*; U.S. Geological Survey's EROS Data Center: Sioux Falls, SD, USA, 2003. Available online: <https://www.usgs.gov/media/files/preliminaryassessment-value-landsat-7-etm-slc-data> (accessed on 15 April 2021).
19. Irons, J.R.; Dwyer, J.L.; Barsi, J.A. The next Landsat satellite: The Landsat data continuity mission. *Remote Sens. Environ.* **2012**, *122*, 11–21. [[CrossRef](#)]
20. Xiong, X.; Sun, J.; Xie, X.; Barnes, W.L.; Salomonson, V.V. On-orbit calibration and performance of Aqua MODIS reflective solar bands. *IEEE Trans. Geosci. Remote Sens.* **2009**, *48*, 535–546. [[CrossRef](#)]
21. Xiong, X.; Chiang, K.-F.; Wu, A.; Barnes, W.L.; Guenther, B.; Salomonson, V.V. Multiyear on-orbit calibration and performance of Terra MODIS thermal emissive bands. *IEEE Trans. Geosci. Remote Sens.* **2008**, *46*, 1790–1803. [[CrossRef](#)]
22. Drusch, M.; Del Bello, U.; Carlier, S.; Colin, O.; Fernandez, V.; Gascon, F.; Hoersch, B.; Isola, C.; Laberinti, P.; Martimort, P. Sentinel-2: ESA's optical high-resolution mission for GMES operational services. *Remote Sens. Environ.* **2012**, *120*, 25–36. [[CrossRef](#)]
23. Barsi, J.A.; Alhammoud, B.; Czaplá-Myers, J.; Gascon, F.; Haque, M.O.; Kaewmanee, M.; Leigh, L.; Markham, B.L. Sentinel-2A MSI and Landsat-8 OLI radiometric cross comparison over desert sites. *Eur. J. Remote Sens.* **2018**, *51*, 822–837. [[CrossRef](#)]
24. Guo, Y.; Li, L.; Jin, L.; Wang, K. Study on cloud processing methods with MODIS data. In Proceedings of the 2013 5th IEEE International Symposium on Microwave, Antenna, Propagation and EMC Technologies for Wireless Communications, Chengdu, China, 29–31 October 2013; pp. 694–696. [[CrossRef](#)]
25. Shrestha, M.; Hasan, N.; Leigh, L.; Helder, D. Derivation of Hyperspectral Profile of Extended Pseudo Invariant Calibration Sites (EPICS) for Use in Sensor Calibration. *Remote Sens.* **2019**, *11*, 2279. [[CrossRef](#)]
26. Jing, X.; Leigh, L.; Helder, D.; Pinto, C.T.; Aaron, D. Lifetime absolute calibration of the EO-1 Hyperion sensor and its validation. *IEEE Trans. Geosci. Remote Sens.* **2019**, *57*, 9466–9475. [[CrossRef](#)]
27. Collings, S.; Caccetta, P.; Campbell, N.; Wu, X. Techniques for BRDF correction of hyperspectral mosaics. *IEEE Trans. Geosci. Remote Sens.* **2010**, *48*, 3733–3746. [[CrossRef](#)]
28. Helder, D.; Thome, K.J.; Mishra, N.; Chander, G.; Xiong, X.; Angal, A.; Choi, T. Absolute radiometric calibration of Landsat using a pseudo invariant calibration site. *IEEE Trans. Geosci. Remote Sens.* **2013**, *51*, 1360–1369. [[CrossRef](#)]
29. Farhad, M.; Kaewmanee, M.; Leigh, L.; Helder, D. Radiometric cross calibration and validation using 4 angle BRDF model between landsat 8 and sentinel 2A. *Remote Sens.* **2020**, *12*, 806. [[CrossRef](#)]
30. Kaewmanee, M. Pseudo Invariant Calibration Sites: PICS Evolution. In Proceedings of the CALCON 2018, Logan, UT, USA, 18–20 June 2018.
31. Savitzky, A.; Golay, M.J. Smoothing and differentiation of data by simplified least squares procedures. *Anal. Chem.* **1964**, *36*, 1627–1639. [[CrossRef](#)]
32. Taubenbock-Taubenbock, H.; Habermeyer, M.; Roth, A.; Dech, S. Automated allocation of highly structured urban areas in homogeneous zones from remote sensing data by Savitzky–Golay filtering and curve sketching. *IEEE Geosci. Remote Sens. Lett.* **2006**, *3*, 532–536. [[CrossRef](#)]

33. Pinto, C.T.; Ponzoni, F.J.; Castro, R.M.; Leigh, L.; Kaewmanee, M.; Aaron, D.; Helder, D. Evaluation of the uncertainty in the spectral band adjustment factor (SBAF) for cross-calibration using Monte Carlo simulation. *Remote Sens. Lett.* **2016**, *7*, 837–846. [[CrossRef](#)]
34. Czapla-Myers, J.; McCorkel, J.; Anderson, N.; Thome, K.; Biggar, S.; Helder, D.; Aaron, D.; Leigh, L.; Mishra, N. The ground-based absolute radiometric calibration of Landsat 8 OLI. *Remote Sens.* **2015**, *7*, 600–626. [[CrossRef](#)]
35. Francesconi, B.; Neveu-VanMalle, M.; Espeset, A.; Alhammoud, B.; Bouzinac, C.; Clerc, S.; Gascon, F. Image quality validation of sentinel 2 level-1 products: Performance status at the beginning of the constellation routine phase. In Proceedings of the Sensors, Systems, and Next-Generation Satellites XXI, Warsaw, Poland, 11–14 September 2017; pp. 44–61. [[CrossRef](#)]
36. Choi, J.; Xiong, X.; Mishra, N.; Helder, D.; Angal, A. Absolute Calibration of Optical Satellite Sensors Using Libya 4 Pseudo Invariant Calibration Site. *Remote Sens.* **2014**, *6*, 1327–1346. [[CrossRef](#)]
37. Angal, A.; Xiong, X.; Helder, D.; Kaewmanee, M.; Leigh, L. Assessing the calibration differences in the reflective solar bands of Terra MODIS and Landsat-7 enhanced thematic mapper plus. *J. Appl. Remote Sens.* **2018**, *12*, 044002. [[CrossRef](#)]
38. Xiong, X.; Angal, A.; Li, Y.; Twedt, K. Improvements of on-orbit characterization of Terra MODIS short-wave infrared spectral bands out-of-band responses. *J. Appl. Remote Sens.* **2020**, *14*, 047503. [[CrossRef](#)]